ENGINEERING RESEARCH INSTITUTE
UNIVERSITY OF MICHIGAN
ANN ARBOR

OPERATION OF INTERDIGITAL MAGNETRONS IN THE ZERO ORDER MODE

Technical Report No. 2
Electron Tube Laboratory
Department of Electrical Engineering

BY

H. W. WELCH, JR.

G. R. BREWER

Approved By:

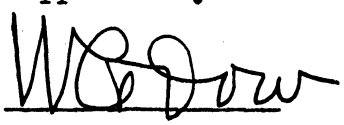

W. G. Dow

Project M694

For

CONTRACT NO. W-36-039 sc-32245
SIGNAL CORPS, DEPARTMENT OF THE ARMY
DEPARTMENT OF ARMY PROJECT NO. 399-13-022
SIGNAL CORPS PROJECT NO. 112B-0

May 23, 1949

TABLE OF CONTENTS

PERSONNEL OF UNIVERSITY OF MICHIGAN
ELECTRON TUBE LABORATORY

Scientific and Engineering Personnel

W. G. Dow	Professor of Electrical Engineering	Supervisor
H. W. Welch	Research Physicist	Full time
J. R. Black	Research Engineer	Full time
G. Hok	Research Engineer	1/4 time
G. R. Brewer	Research Assistant	1/2 time
R. K. Brown*	Research Engineer	1/2 time
R. Callahan*	Research Associate, Student	1/2 time
C. K. Birdsall*	Research Assistant, Student	1/3 time

Service Personnel

V. R. Burris	Machine Shop Foreman	Full time
R. F. Steiner	Assembly Technician	Full time
Mrs. G. R. Merithew	Draftsman and Illustrator	3/4 time
D. L. McCormick	Machinist	1/2 time
E. H. Kayser	Machinist	1/2 time

* These personnel were involved in compilation of material included in this report, but are no longer with the project.

ABSTRACT

This report presents theory and experimental results pertaining to operation of interdigital magnetrons in the zero order mode at power levels from 100 to 500 watts. An analysis of the properties of the cathode circuit which are important to this type of operation is given. Practical problems of design are discussed. Experimental results on four different models are summarized and shown to agree very well with the theory. Alternative structures are proposed which are based on the interdigital magnetron principle.

ACKNOWLEDGMENTS

Every member of the staff of the University of Michigan Tube Laboratory was involved in the preparation of the material used in this report. Most of the details of constructional design, the design of the cathode, and actual assembly and processing of the magnetrons were the responsibility of Mr. J. R. Black. The work was supervised by Professor W. G. Dow who was originally responsible for the emphasis on the interdigital type of structure in this laboratory. Thanks are given to Mr. J. F. Hull of Evans Signal Laboratory for helpful suggestions made early in the development of the project.

OPERATION OF INTERDIGITAL MAGNETRONS IN THE ZERO ORDER MODE

1. INTRODUCTION

The interdigital magnetron has for various reasons been by-passed in advanced development at high power levels. These reasons are in part historical and in part connected with inherent features of the interdigital type of structure which make it particularly adaptable to some low power applications. Wartime emphasis on the interdigital structure was not begun until the vane magnetron was already performing efficiently in practical applications. Initial emphasis was on small low power tubes with glass envelopes for use in external resonant cavity structures. Higher order modes were used because the zero order mode failed to produce efficient operation. In all cases, two or more slightly different frequencies were developed in higher order modes. Much of the emphasis dealt with the suppression of one of these.

The reason for inefficient operation in the zero order mode has since been discovered.(1) This reason is simple in principle. Power can be developed in the zero order mode, but because of inherent characteristics of the interdigital magnetron, there is very strong coupling of power out through

---

(1) Hull, J. F. and Randalls, A. W., "High Power Interdigital Magnetrons", Proc. IRE, Vol. 36, No. 11, November 1948, pp. 1357-1363. This information was privately communicated to the Michigan Group by Mr. Hull in March, 1947.

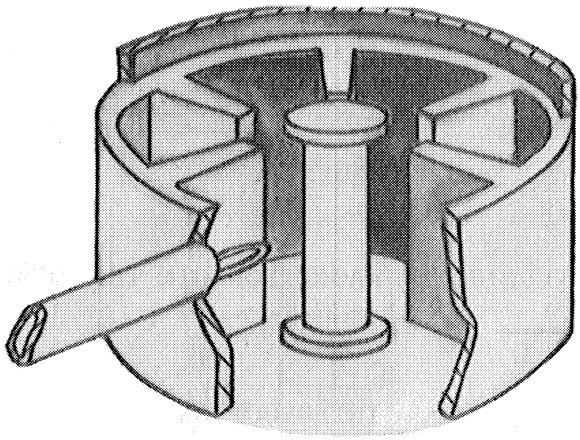

a
VANE TYPE MAGNETRON

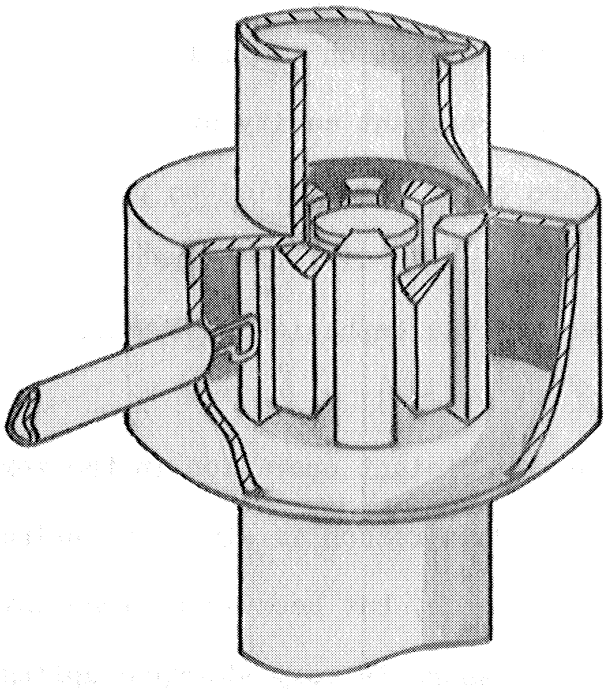

b
INTERDIGITAL MAGNETRON

FIG. 2.1 COMPARISON OF INTERDIGITAL MAGNETRON STRUCTURE WITH VANE TYPE STRUCTURE

the cathode circuit. Efficient operation (over 70 per cent) is obtained by preventing the escape of power with a resonant choke and by-pass combination, or by decreasing the coupling by modification of the interdigital tooth structure. The zero order mode is particularly applicable to structures which hold promise as frequency modulation magnetrons. The Michigan Group has therefore given considerable time and effort to the achievement of a better understanding of operation in this mode. Compared to higher order modes the zero order mode is unique in many characteristics and deserves separate attention. Particular emphasis has been given in this laboratory to both theoretical and experimental analysis of the problem of coupling to the cathode circuit. Seven operable tubes including three basically different models have been built. Two of the models have thus far been operated in the desired mode. One of these operated with efficiency over 70 per cent. The cathode by-pass of the inoperable model is being revised and it is expected that satisfactory operation will be obtained.

The interdigital magnetron anode is quite adaptable to a variety of resonant circuits. Three alternative structures have been studied. One of these structures has been built into a frequency modulation magnetron and initial tests gave encouraging results with power output in the expected mode. Further development is planned on this structure and others, both conventional and unconventional in design.

2. GENERAL CHARACTERISTICS OF THE INTERDIGITAL MAGNETRON

For purposes of comparison, Figure 2.1 shows a sectional view of a vane magnetron and an interdigital magnetron. In both cases, the field distribution in the cavities for the fundamental mode is such that the electric

fields are oppositely directed between successive anode segments. A method for analyzing the fundamental or zero order mode of the interdigital structure is given in the next section. Unless expressly stated, this mode is the subject of all following discussion.

The important feature of the interdigital magnetron is that the function of the anode segments in the resonant circuit is in most cases that of a capacitance lumped across a single simple cavity. In the unstrapped vane magnetron the N anode segments are attached to N resonant circuits. A number of resonances, close together in frequency, are thereby necessarily produced. If the magnetron is heavily strapped to separate these resonances, the structure becomes electrically similar in principle to the interdigital structure but maintains a complex structure mechanically.

Probably the most important advantage of simplifying the function of the anode segments is that the cavity to which they are attached does not necessarily take the form of the flat cylindrical cavity employed in conventional interdigital magnetrons. This allows for much more flexibility in design, making practical without doubt many possibilities which to date have not even been tentatively explored. It is also possible to place the anode segments in a glass envelope to operate as an oscillator tube in external cavities of varied size and shape.(1) Heretofore, this has only been possible with split anode tubes which do not operate satisfactorily at the high frequencies obtainable with the interdigital type (i.e., 10 cm to 5 cm). This feature, if it can be developed further to include high power levels, can

---

(1) For example: the Sylvania tube No. SO 849. Work is also being done on a tube of this type in the University of Illinois Electron Tube Laboratory.

lead to vast simplification of tuning problems. Another feature is that it is possible to include more than one set of anode segments in a single resonant circuit. This is attractive from the point of view of frequency modulation since one set can be used as a generator and one set as a modulator. Most of the activity on the Michigan project has been in this direction.

Another advantage of the interdigital magnetron is in the inherently good mode separation. The mode separation is probably no better than a heavily strapped vane magnetron but as has already been pointed out, the structure with which it is obtained is simpler.

Tuning of interdigital magnetrons is usually accomplished by changing the end capacitance of the anode fingers by moving one set of anode segments axially. Movement is permitted by mounting one anode set on a flexible diaphragm which forms one end wall of the resonant cavity. This method of tuning is not particularly satisfactory in that interaction space geometry is distorted by the process; also, a poor heat conduction path is provided from one set of anode segments. Some low power level tubes have been used with tuning supplied in the cavity but very little thought has been given to the development of improved methods at high power levels. The problem of heat dissipation in the fingers has been considered a limiting feature of interdigital magnetrons. However, proper design of the tooth structure virtually eliminates this objection. The major disadvantage of zero order mode operation is in the difficulty in designing a choke and by-pass combination which works well over the entire tuning range of the tube. This problem has been analyzed to some extent but the detailed design of an operating tube with broad-band choke and by-pass has not been attempted to date.

Figure 4.1 shows a cutaway view of a typical interdigital magnetron constructed for operation in the zero order mode with cathode choke and by-pass sleeves.

3. ZERO ORDER MODE IN THE CAVITY

The principal resonant element employed in the interdigital magnetron is in the form of a cylindrical cavity operating in the TM 10 mode (ℓ is used to designate the order of the mode). This type of cavity together with a representation of the electric and magnetic fields for the zero order mode ($\ell = 0$) is shown in Figure 3.1. It is seen that the only components of field present are E_Z and H_ϕ with no variations in the Z or ϕ directions.

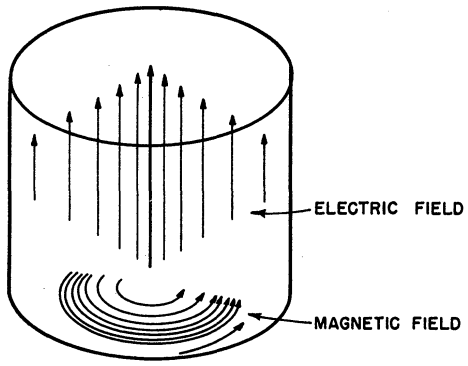

FIG. 3.1 FIELD CONFIGURATION IN CYLINDRICAL CAVITY - TM_{010} MODE

In order to provide components of electric field with which electrons can interact to produce oscillations, "teeth" are inserted, joined alternately to the upper and lower faces of the cavity. A drawing of the modified cavity together with a qualitative sketch of the fields existing around the teeth are shown in Figure 3.2. It is seen that the fields in the interaction space are similar to those existing in a vane or hole and slot magnetron when operated in the π mode. Due to its construction, of course, the interdigital cavity can present only π mode fields in the interaction space.

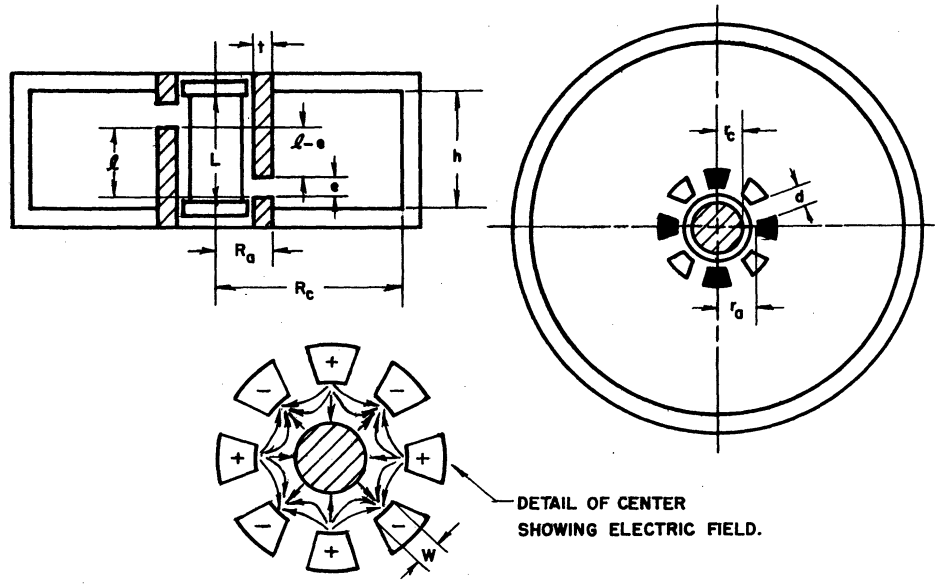

FIG. 3.2 VIEW OF CAVITY SHOWING TEETH AND ELECTRIC FIELD AROUND TEETH.

The field configurations in such a cavity prompt one to consider it as a transmission line in which the guided wave is propagated radially. The line is considered as terminated in a conducting surface at the outer radius R_c and loaded by the lumped capacitance of the "teeth" at the inner radius R_a. The solution[1] of the field equations for such a structure, subject to the boundary conditions just imposed, yield the impedance looking outward from radius R_a into the transmission line as

$$Z_{in} = -j \frac{hZ_{oa}}{2\pi R_a} \frac{\sin(\theta_a - \theta_c)}{\cos(\psi_a - \theta_c)} \qquad (3.1)$$

where Z_{oa} is the characteristic impedance of the line defined at radius R_a.

$$\theta_a = f\left(\frac{2\pi R_a}{\lambda}\right) \qquad \theta_c = f\left(\frac{2\pi R_c}{\lambda}\right) \qquad \psi_a = g\left(\frac{2\pi R_a}{\lambda}\right)$$

where the functional relationships are given by means of the graphs in Figure 3.3.

The condition for resonance is obviously

---

(1) Ramo and Whinnery, "Fields and Waves in Modern Radio", John Wiley and Sons, pp. 355 and 407, 1944.

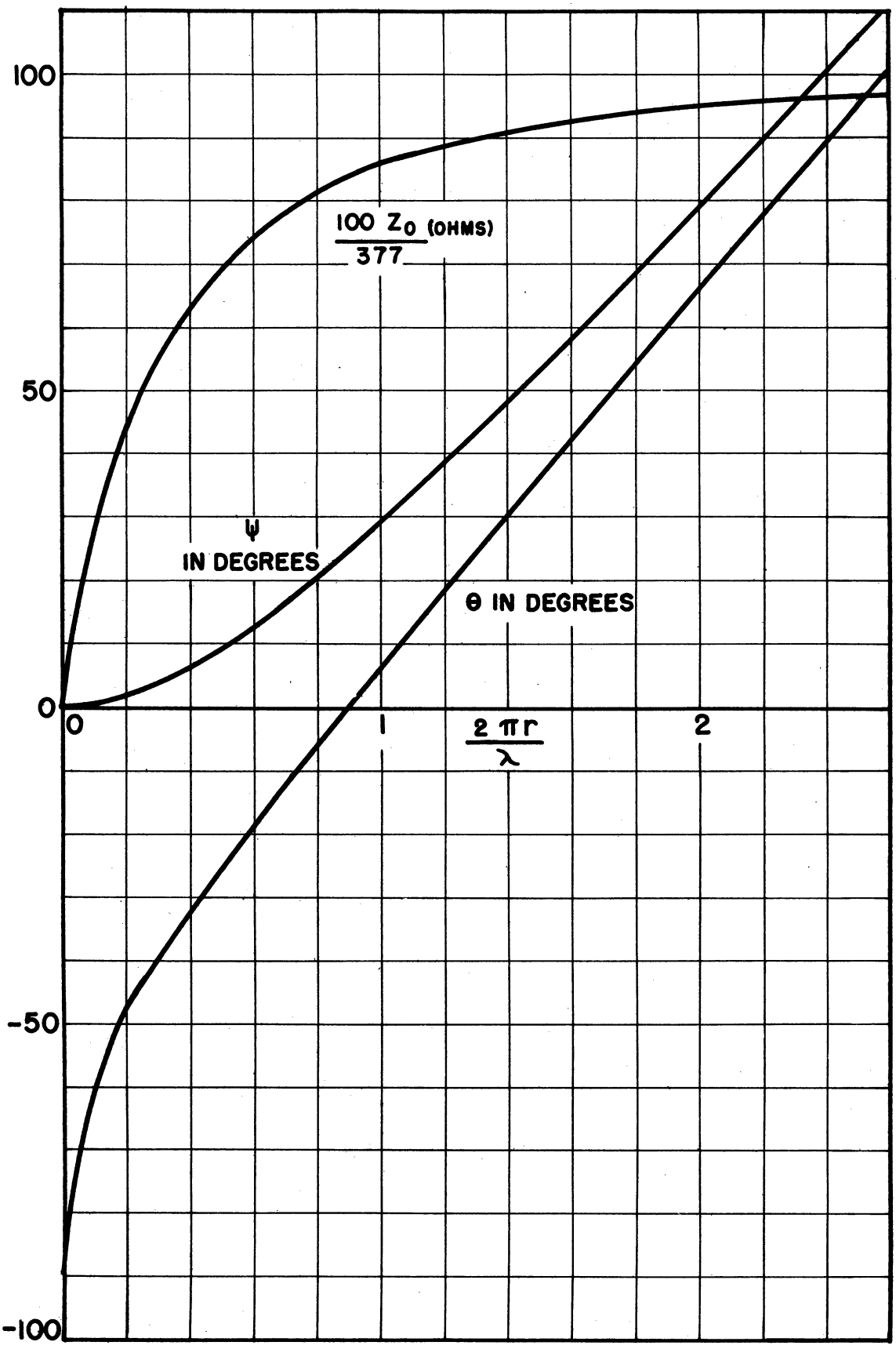

FIG. 3.3 RADIAL TRANSMISSION LINE QUANTITIES

$$Z_{in} = \frac{j\lambda}{2\pi c C_A} \tag{3.2}$$

where C_A is the lumped tooth capacitance. This is based on the assumptions which seem to be reasonably accurate for zero order mode calculations, that the teeth are essentially non-inductive and that the capacitance is lumped rather than distributed. So that, combining (3.1) and (3.2) and solving for θ_c

$$\theta_c = \tan^{-1} \frac{\sin \theta_a - \frac{\lambda R_a}{c C_A Z_{oah}} \cos \psi_a}{\cos \theta_a - \frac{\lambda R_a}{c C_A Z_{oah}} \sin \psi_a} \tag{3.3}$$

Using this formula and the curves of Figure 3.3, a cavity can be designed to resonate at the desired wavelength if the anode capacitance is known.

In order to find the capacitance C_A of the interlocking tooth structure, a section of which is shown in Figure 3.4a, the ordinary parallel plate formula may be used in the region where the teeth are parallel (region AB of Figure 3.4c) so that in this region

$$C = 2 \frac{\epsilon_o (\ell - 2d) t}{d} \tag{3.4}$$

where t is the thickness of the teeth, and ϵ_o is the dielectric constant of free space. The remaining end portions of the teeth are considered as joined to form the concentric square structure of Figure 3.4b. The capacitance of such a condenser has been found[1] from the distribution of charge on a corner whose sides are equidistant inside another corner to be

$$C = 8 \epsilon_o t \left[1 - \frac{\ln 2}{\pi} \right]$$

---

(1) Thomson, J. J., "Recent Researches in Electricity and Magnetism", Oxford Clarendon Press, pp. 222, 1893.

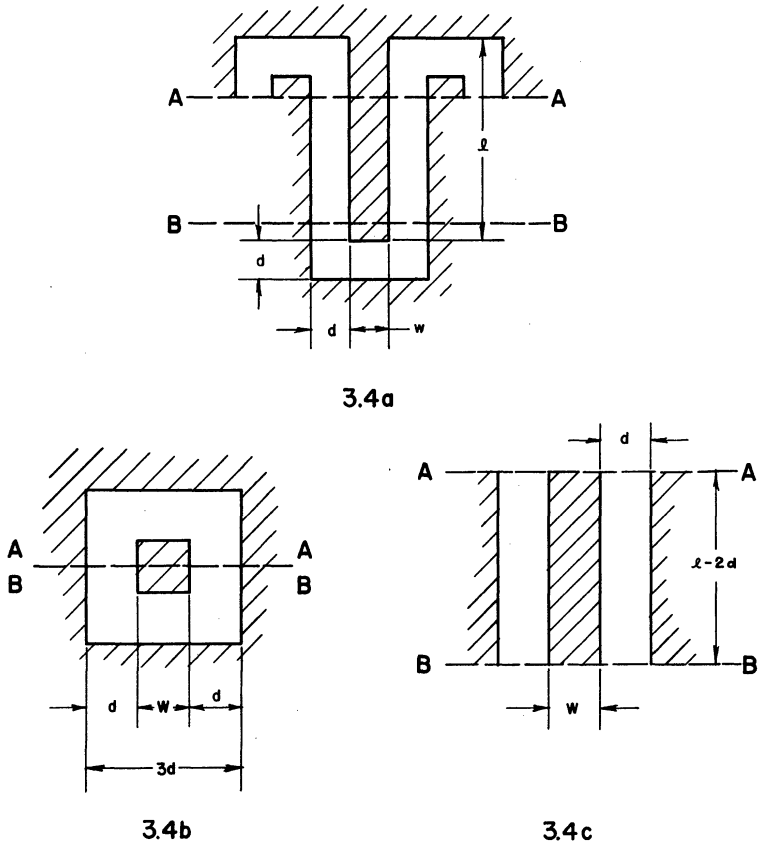

FIG. 3.4 FIGURES USED IN CALCULATING CAPACITANCE OF ANODE STRUCTURE.

the total capacitance of N teeth is then

$$C_A = K \frac{N}{2} \epsilon_o t \left[\frac{\ell - 2d}{d} + 4\left(1 - \frac{\ln 2}{\pi} \right) \right]$$

$$= KN \epsilon_o t \left[\frac{\ell}{d} + 1.12 \right] \text{ farads} \qquad (3.5)$$

where K[1] is a correction factor to compensate for edge effects. Two relations for K, valid for long parallel thin strips, are:

$$K = 1 + \frac{d}{\pi t} \left[1 + \ln \frac{2\pi t}{d} \right] \qquad (3.6)$$

---

(1) Palmer, H. B., "The Capacitance of a Parallel Plate Capacitor by the Schwartz Christoffel Transformation", Trans. AIEE, Vol. 56, No. 3, p. 363, March 1937.

for large values of t/d, and

$$K = \frac{\pi d}{t} \frac{1}{\ln(\frac{4d}{t})} \tag{3.7}$$

for small values of t/d.

A somewhat more accurate expression for the tooth capacitance has been derived[1] from the work of J. J. Thomson[2].

Thomson has shown that the total charge between points 1 and 2 on a semi-infinite plate between two infinite planes (see Figure 3.5) is

$$\epsilon_o \left[\frac{4x}{d} + \frac{2}{\pi} \left(\frac{w + d}{d} \ln(\frac{2d + w}{d}) + \ln \frac{w(2d + w)}{d^2} \right) \right] \tag{3.8}$$

per unit length for unit potential difference between the semi-infinite plate and the two planes. It is seen that the first term of Equation (3.8) is just the parallel plate formula so that use of this relation tacitly assumes the fields between the plate and the planes to be uniform; this will be nearly true when t>d. The second term of Equation (3.8) represents the fringing field, and if we assume this to be the same on the sides of the rectangular bar of Figure 3.5b as on the end of the semi-infinite plate of Figure 3.5a, the total charge on the bar between planes is approximately

$$\epsilon_o \left[\frac{4t}{d} \quad \frac{4}{\pi} \left(\frac{w + d}{d} \ln \frac{2d + w}{d} + \ln \frac{w(2d + w)}{d^2} \right) \right]$$

Since this relation is for unit potential difference, it also expresses the capacitance between bar and planes, per unit length. Then the capacitance between a pair of bars, shown in Figure 3.5c is:

$$\epsilon_o \frac{2t}{d} \left[1 + \frac{d}{\pi t} \left(\frac{w + d}{d} \ln \frac{2d + w}{d} + \ln \frac{w(2d + w)}{d^2} \right) \right] \tag{3.9}$$

---

(1) "Obstacle Loaded Cylindrical Cavities with Application to the Interdigital Magnetron", ONR Tech. Report No. 60, Cruft Laboratory, Harvard University, November 1, 1948.

(2) Thomson, J. J., loc. cit., p. 219.

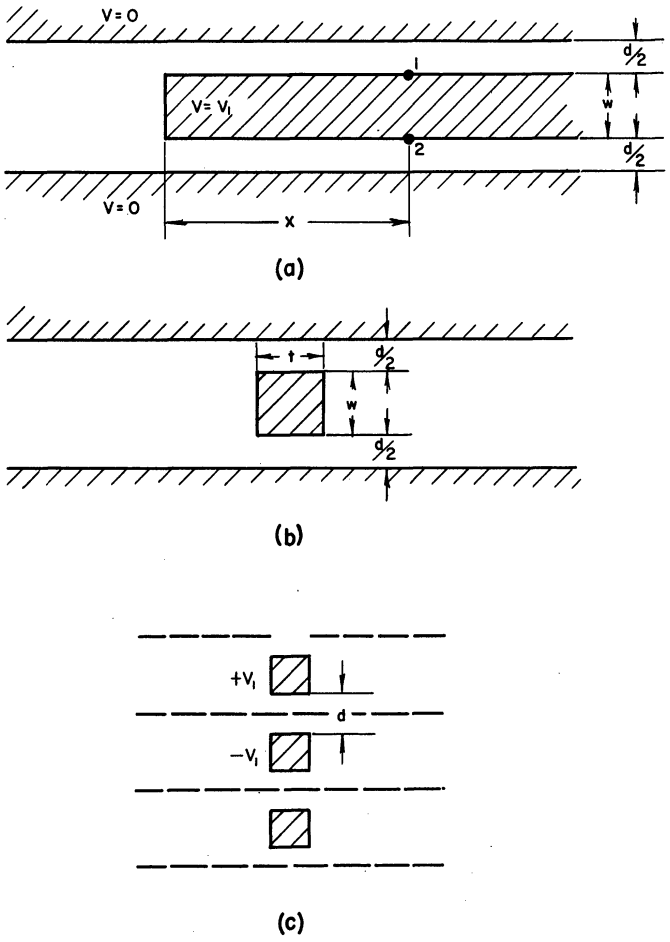

FIG. 3.5 FIGURES USED IN DERIVATION OF TOOTH CAPACITANCE EQUATION — 3.10

The capacitance per bar is one-half of this result.

In order to apply these results to the calculation of interdigital anode capacitance, we assume that the fringing correction, found as the second term of Equation (3.9), is applicable to the end region of the tooth (Figure 3.4b) as well as to the parallel portions. We then have for the correction term to be applied to Equation (3.5)

$$K = 1 + \frac{d}{\pi t}\left[\frac{w+d}{d}\ln\frac{2d+w}{d} + \ln\frac{w(2d+w)}{d^2}\right] \qquad (3.10)$$

While this equation is derived to give the correction due to fringing fields per unit length, it may be applied directly to Equation (3.5) which contains the length. A special case, representative of most interdigital magnetrons,

is that when w = d; then the expression for the total tooth capacitance reduces to:

$$C_A = N \epsilon_o t \left[\frac{\ell}{d} + 1.12\right]\left[1 + 1.05 \frac{d}{t}\right] \qquad (3.11)$$

As seen from Figure 3.4, those formulae are valid only when the spacing at end of teeth is equal to the spacing between teeth (d). A correction factor accounting for the effect of the cathode may also be added. This correction is usually of the order of 5 or 6 per cent of the total capacitance.

By the use of the result of Equation (3.11) for a given cavity in Equation (3.3), the resonant wavelength may be computed. It is seen from Equation (3.3) that an explicit solution for resonant wavelength is difficult so that the usual procedure in design is to determine the outer cavity radius, R_c. However, if the resonant wavelength of a given cavity is required, it may be obtained implicitly from the values of R_c.

It should be pointed out here that the condition for resonance given by Equation (3.2) is based on several assumptions. That is, Equation (3.2) merely expresses an equality between the input impedance of the radial transmission line and the lumped capacitive reactance of the teeth. Except for a relatively small correction for fringing, the input impedance of the transmission line, defined at radius R_a, should be given correctly by Equation (3.1). However, there is an error in considering the capacitance of the teeth to be lumped at radius R_a. This assumption will be an increasingly larger error as the teeth are made thicker relative to the cavity depth $R_c - R_a$ since in this condition the radial field distribution in the teeth must be considered. Data will be presented in Section 7 to demonstrate this effect.

Experimental results showing the effect of variation in the outer cavity diameter on the resonant wavelength of the cavity alone are given in

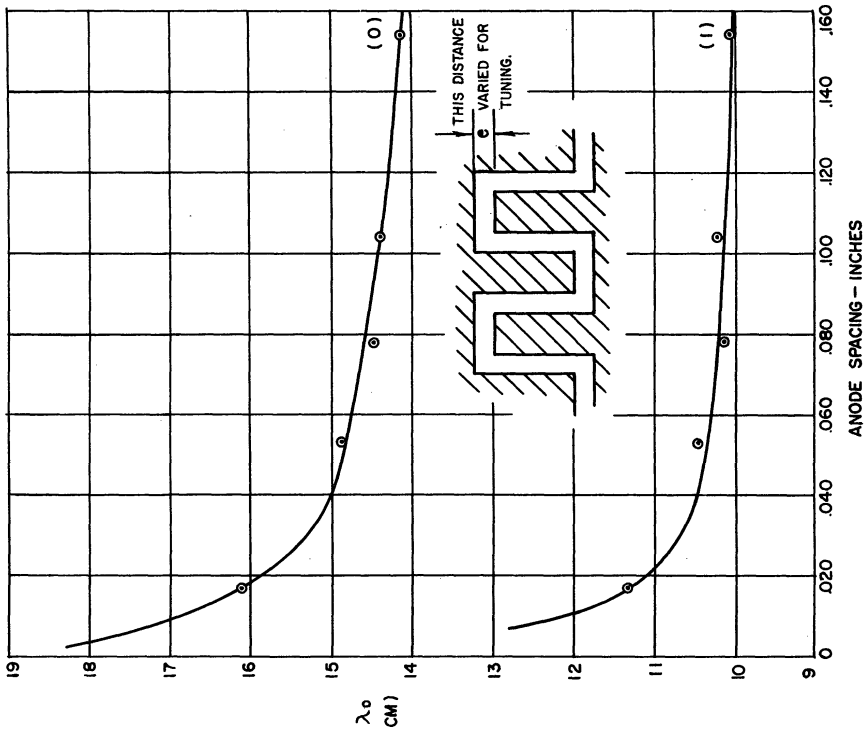

FIG. 3.7 TYPICAL TUNING CURVES OF ZERO AND FIRST ORDER MODES.

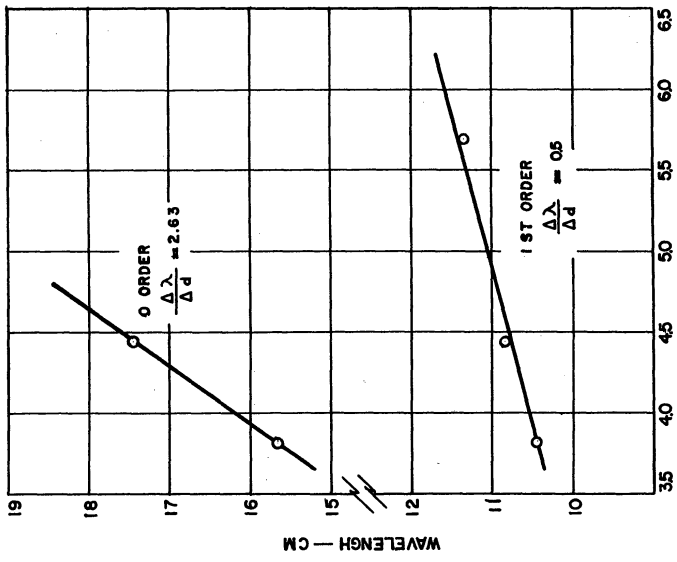

FIG. 3.6 EFFECT OF CAVITY DIAMETER ON RESONANT WAVELENGTH OF ZERO AND FIRST ORDER MODES.

Figure 3.6. The slope of the line corresponding to the zero order mode is seen to be considerably greater than that for the first order mode. This can be explained from the variation in field intensities with radius for the two modes. In the first order mode the magnetic field decreases in intensity much more rapidly, that is, it is more concentrated near the teeth. The resonant wavelength of the zero order mode would thus be expected to be more susceptible to variations in cavity diameter, as shown.

Typical tuning curves, showing the variation in cavity resonant wavelength with tooth capacitance, are shown in Figure 3.7. The tooth capacitance is varied by changing the anode spacing, that is, the distance from end of tooth to the base of cavity. In the case of teeth which are of the same cross-section along their length, the principal effect on capacitance (C_A) will be the change in end spacing so that the capacitance variation with anode spacing would be expected to be approximately a rectangular hyperbola. This limits the tuning range to the region where the anode spacing is small. In order to increase the tuning at large anode spacings, various modifications have been tried. For example, tapering the teeth as shown in Figure 3.8 will result in a tuning curve whose flat portion slopes downward, resulting in increased tuning range.

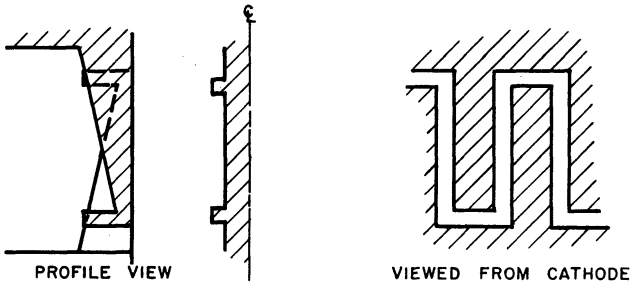

FIG. 3.8 SHOWING TAPERED TOOTH DESIGN FOR INCREASED TUNING RANGE.

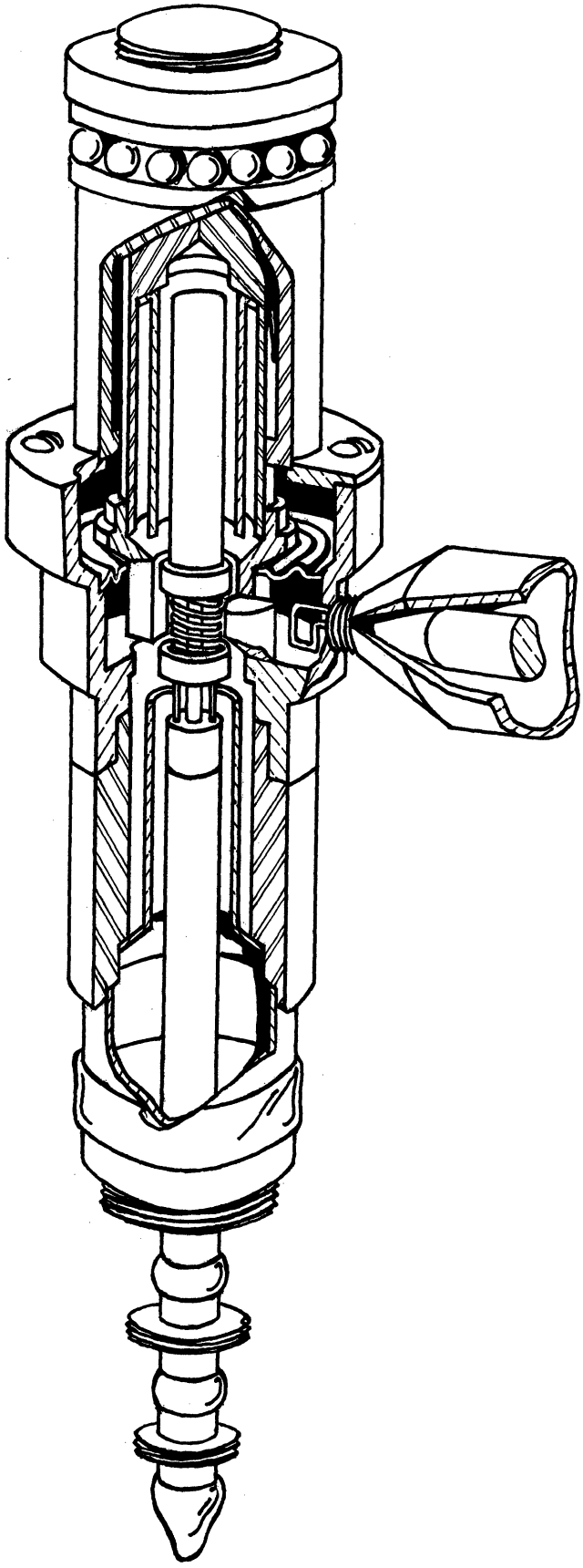

FIG. 4.1 SECTIONAL VIEW
INTERDIGITAL MAGNETRON

Experimental determination of the field patterns in such a cavity as considered here has been made by inserting a probe into holes placed around the surface of a brass model cavity. The relative magnitudes of the fields can be found for various modes which exist in the cavity. Distributions in the interaction space have been checked by means of rotating probe techniques. Some of these measurements on higher order modes are described in Section 5.

4. EFFECT OF THE CATHODE STRUCTURE

Figure 4.1 shows a cross-section drawing of a typical interdigital magnetron.

Figure 4.2 shows a cold test model constructed to approximate with a simplified geometry the complete r-f circuit of such a tube. This permits

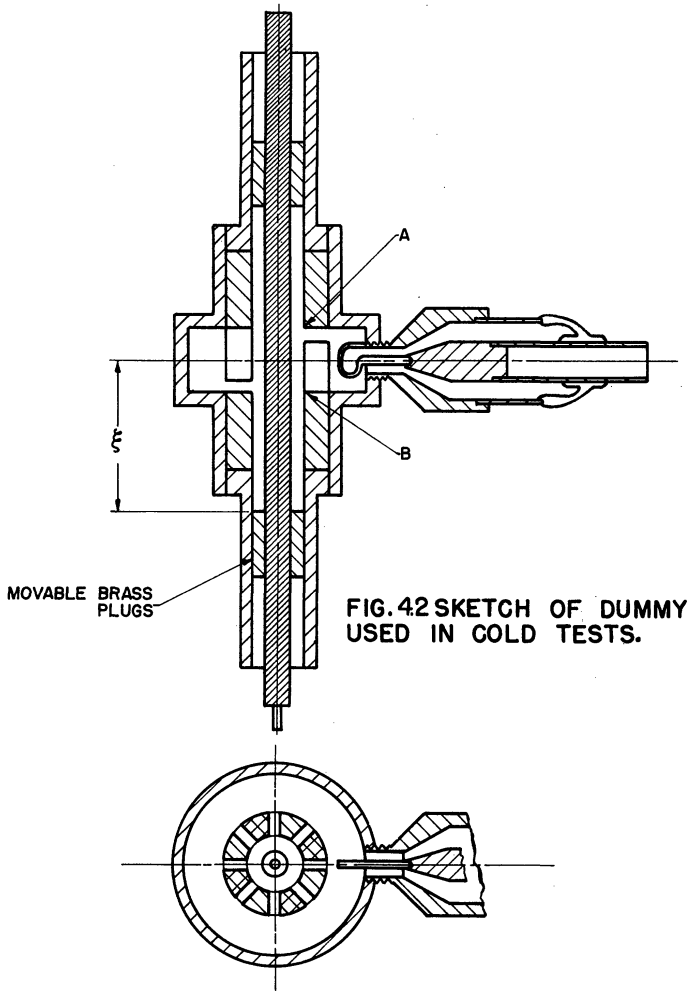

FIG. 4.2 SKETCH OF DUMMY MAGNETRON USED IN COLD TESTS.

experimental investigation of a structure for which a relatively simple theory can be developed. As stated previously, the cavity resonates in such a mode that at any given instant one side of the cavity (point A) may be at an r-f potential of $+e_a$ and the other side (point B) $-e_a$ with reference to a neutral point. Thus, in the zero order mode, there will exist a voltage across the ends of the coaxial transmission lines formed by the cathode structure. Due to the configuration of fields in the cavity when in the higher order modes, this voltage will, to a large extent, balance so that very little coupling will exist between the fields in the cavity and in the cathode structure.

However, as will be shown later, this coupling is so strong when the fields in the cavity correspond to the zero order mode that the complete r-f circuit of the interdigital magnetron must be represented by an equivalent circuit such as that shown in Figure 4.3. The parallel circuit composed

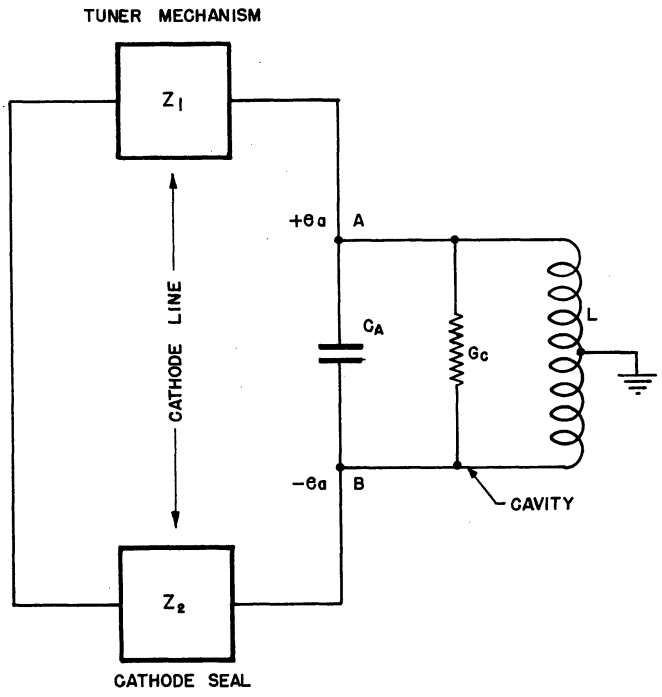

FIG. 4.3
EQUIVALENT CIRCUIT OF INTERDIGITAL MAGNETRON (0 ORDER MODE)

of L, C_A and G_c represents the cavity, while Z_1 and Z_2 represent the impedances presented by the coaxial transmission line at the face of the cavity. Then considering the model shown in Figure 4.2:

$$Z_1 = Z_o \tan\frac{2\pi}{\lambda}\xi_1$$

$$Z_2 = Z_o \tan\frac{2\pi}{\lambda}\xi_2$$

where ξ_1 and ξ_2 are the distances from the shorting plugs to the faces of cavity. In the case of symmetrically placed plugs, $\xi_1 = \xi_2 = \xi - \frac{h}{2}$.

Using this equivalent circuit the condition for resonance in the system becomes

$$\frac{\lambda^2}{2\pi cL} + \frac{\lambda}{Z_o \tan\frac{2\pi}{\lambda}\xi_1 + Z_o \tan\frac{2\pi}{\lambda}\xi_2} - 2\pi c C_A = 0 \qquad (4.1)$$

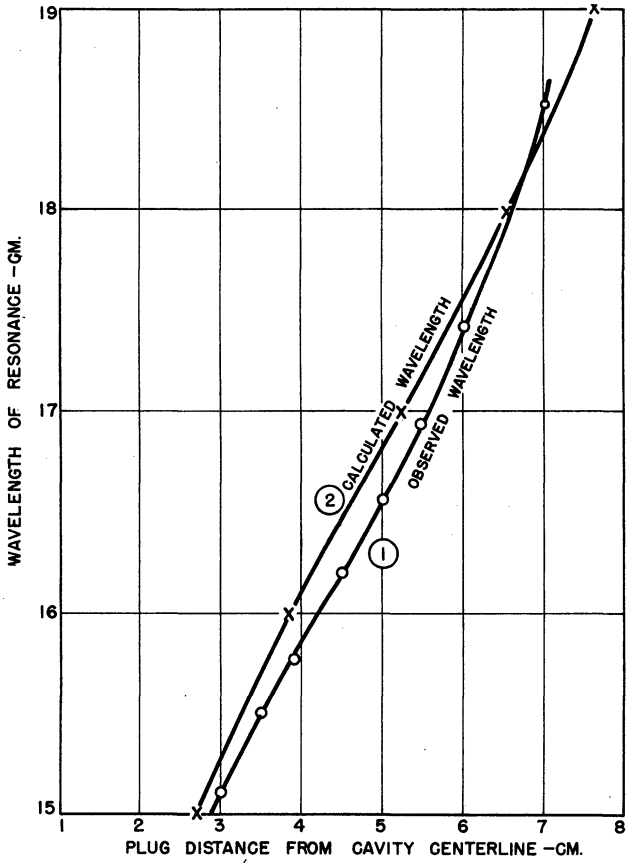

FIG. 4.4
COMPARISON OF CALCULATED AND OBSERVED EFFECT OF CHOKE LENGTH

Using this relation, a curve of resonant wavelength versus plug position can be plotted and compared with experimental data. This is done in Figure 4.4 where it is seen that the agreement between theory and experiment is good, providing confirmation of our assumed equivalent circuit. Some error must exist since the reactance looking into the radial transmission line is assumed to have the same frequency characteristic as the reactance of an inductance L. L is defined for resonance without the presence of the cathode.

In the actual tube, of course, the shorting plugs must be replaced by a choke and by-pass combination. In order to determine the relation between the impedance presented at the cavity by the choke and by-pass, relative

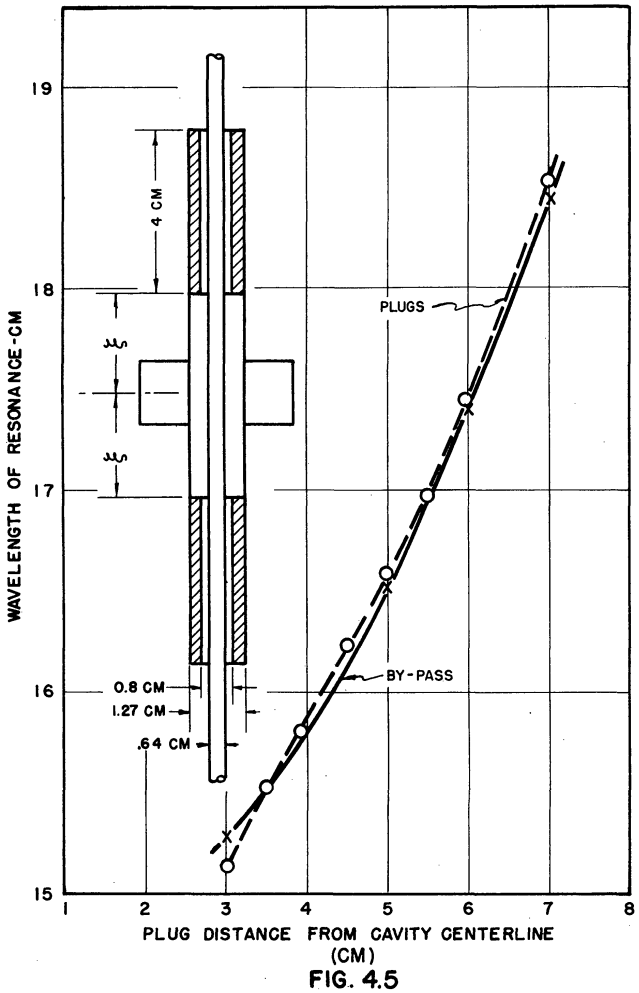

FIG. 4.5
COMPARISON BETWEEN SHORTING PLUGS
AND CATHODE BY-PASS

to that by the shorting plugs, the wavelength versus choke position was measured and is shown in Figure 4.5. It is seen that within experimental error the two curves are coincident for purposes of calculation of resonant wavelength, indicating that closely spaced by-pass sleeves are equivalent to shorting plugs over a wide range of wavelength even though they are $\lambda/4$ long at only one value of wavelength. There is an effect upon the Q of the system which will be outlined below.

As mentioned before, due to the configuration of fields in the cavity and interaction space when operating in the first order mode, it is to be expected that no coupling would exist to the cathode line. Any coupling present, therefore, would be due to dissymmetries or unbalance in the

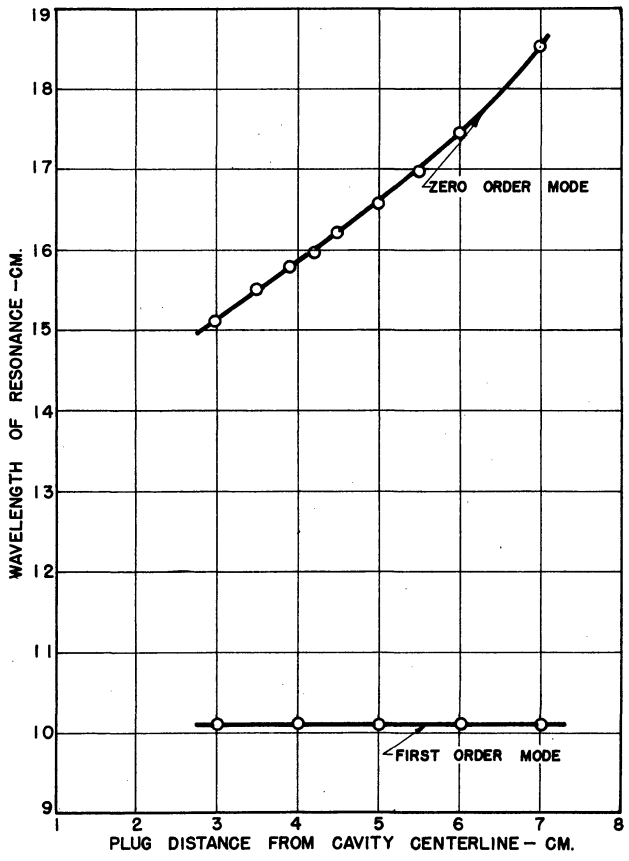

FIG. 4.6

SHOWING EFFECT OF CHOKE LENGTH ON ZERO ORDER AND FIRST ORDER MODE. THIS CONFIRMS LACK OF COUPLING TO CATHODE FOR FIRST ORDER MODE.

fields. That such coupling is in fact extremely small for the first order mode is shown in Figure 4.6 where comparison can be made with the very considerable wavelength shift in the zero order mode.

As can be seen from Figure 4.1, any power which is transmitted down the cathode line may pass through the glass seal and be radiated from the filament structure. This radiation or coupling from the end of the cathode will result in the presence of a resistive component in the impedance Z_2 (Figure 4.3). It is obviously undesirable that any appreciable portion of the power generated in the cavity be dissipated in this resistance. In order to prevent this, the choke and by-pass must be properly designed and placed along the cathode line. A relation can be derived to enable the proper design of a cathode choke and by-pass as follows. Referring to Figure 4.7, Z_2 is thought of as the lumped impedance at the cavity. Z_3 is the actual impedance

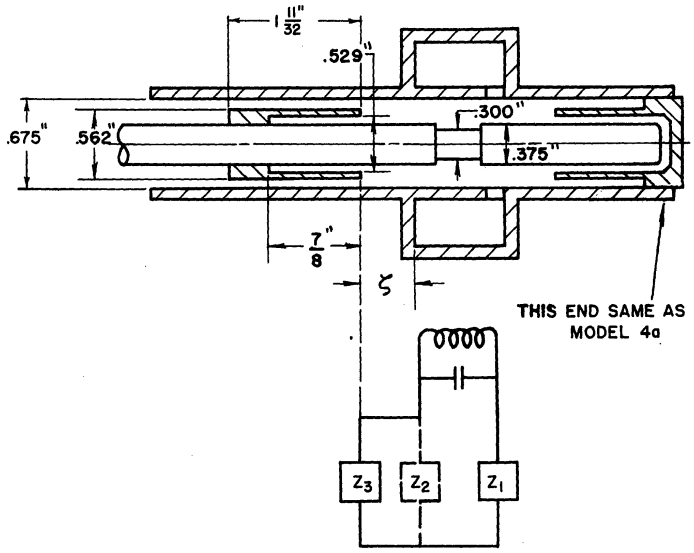

FIG. 4.7 SCHEMATIC AND EQUIVALENT CIRCUIT OF INTERDIGITAL MAGNETRON.

seen looking into the input of the choke and by-pass sections in series. Then

$$Z_2 = Z_o \left[\frac{Z_3 \cos \beta\zeta + j Z_o \sin \beta\zeta}{Z_o \cos \beta\zeta + j Z_3 \sin \beta\zeta} \right] \tag{4.2}$$

The total admittance of the circuit as seen from points A-B is then

$$Y_t = G_c + j2\delta\sqrt{\frac{C_A}{L}} + \frac{1}{jX_1 + R_2 + jX_2} \tag{4.3}$$

where we assume $Z_1 = jX_1$ and let $Z_2 = R_2 + jX_2$.

$$Y_t = G_t + jB_t$$

$$G_t = G_c + \frac{R_2}{R_2^2 + (X_1 + X_2)^2} \tag{4.4}$$

$$B_t = B_{cavity} + B_{cathode}$$

$$B_t = 2\delta\sqrt{\frac{C_t}{L}} \quad \frac{X_1 + X_2}{R_2^2 + (X_1 + X_2)^2}$$

and the Q of the circuit, considering the loading to be due to dissipation in G_c and R_2, can be written:

$$Q = \frac{1}{2}\frac{\Sigma|B|}{G_t} = \frac{1}{2} \frac{2\delta\sqrt{\frac{C_t}{L}} + \frac{X_1 + X_2}{R_2^2 + (X_1 + X_2)^2}}{G_c + \frac{R_2}{R_2^2 + (X_1 + X_2)^2}} \tag{4.5}$$

It is seen that Q will be a maximum with respect to variations in X_2 when $X_2 = \infty$; that is $B_2 = 0$. From Equation (4.2) this condition will be fulfilled when

$$-B_3 Y_o(\cos^2\beta\zeta - \sin^2\beta\zeta) - (B_3^2 - Y_o^2 + G_3^2)(\sin \beta\zeta \cos \beta\zeta) = 0 \tag{4.6}$$

If as a first approximation we neglect G_3 in Equation (4.6) and use choke and by-pass dimensions from the model illustrated in Figure 4.7 to evaluate B_3, the optimum distance ζ for maximum Q calculated from Equation

(4.6) is found to be 1.58 cm. The unloaded Q of the cavity and cathode line Q_{ot} (that is, the Q in which dissipation is in G_c and R_2) was then measured as a function of ζ with the result plotted in Figure 4.8. It is seen that the experimentally determined value for maximum Q agrees very well with that calculated above. Equation (4.6) will thus enable the proper placement of any desired choke and by-pass section. The approximately correct position is obtained if the by-pass sleeve is made $\lambda/4$ long and the short from by-

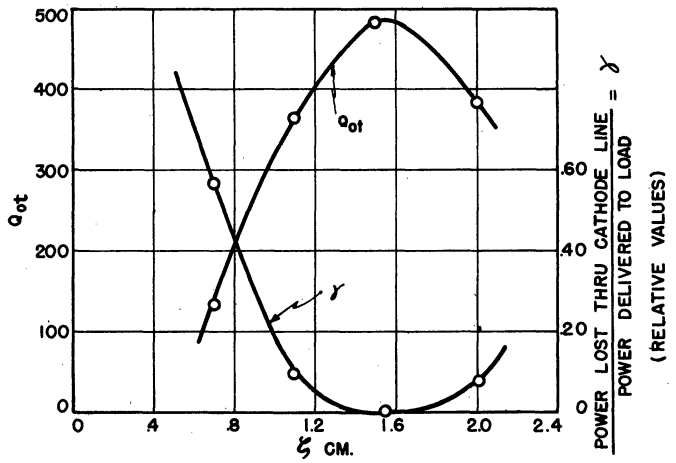

FIG. 4.8
Q OF CAVITY AND CATHODE LINE AS FUNCTION OF CHOKE AND BY-PASS POSITION

pass sleeve to the outer boundary of the cathode line is placed $\lambda/4$ distant from the cavity face. In the case of a tunable tube, it can be placed properly for a wavelength near the center of the tuning range. If the range over which a relatively small amount of power is coupled out the cathode is compared with the tuning ranges of tubes discussed in Section 7, it is plain that wider band choke and by-pass combinations are needed. This will be in part the subject of future development.

In order to provide an illustration of the seriousness of proper by-pass and choke design and placement, let us consider some experimental measurements on a brass tube model.

Unloaded Q with cathode and choke shorted = Q_{oc} = 312

Unloaded Q with cathode and improperly designed choke and by-pass

= Q_{ot} = 134

Loaded Q with cathode and improperly designed choke and by-pass

= Q_{Lt} = 63

$$Q_{ot} = \frac{\text{Energy stored in circuit}}{\text{Power delivered to cavity and cathode line}}$$

$$Q_{oc} = \frac{\text{Energy stored in circuit}}{\text{Power delivered to cavity}}$$

$$Q_{ext\ t} = \frac{\text{Energy stored in circuit}}{\text{Power delivered to load}} = \frac{1}{Q_{Lt}} - \frac{1}{Q_{ot}}$$

Using these definitions then

$$\frac{\text{Power dissipated through cathode line}}{\text{Power delivered to load}} = \frac{1/Q_{ot} - 1/Q_{oc}}{1/Q_{Lt} - 1/Q_{ot}} = 0.53$$

Thus the power dissipated through the cathode line due to radiation, etc., is 53 per cent of the power delivered to the load by way of the coupling loop. If no by-pass sleeve is present, this can be as high as 80 per cent or more, and it can be appreciated that this loss by way of the cathode line is undesirable. In extreme cases, this loss has been sufficient to prevent a tube from oscillating in the zero order mode.

It has thus been established that to prevent loss of power via the cathode line, Z_2 must be made very large. Referring again to the equivalent circuit of Figure 4.3, if we consider that the emitting surface of the cathode is to be maintained at a neutral potential, then to maintain equal r-f voltages between emitting surface and opposite ends of the cavity, Z_1 must be equal to Z_2. Therefore, in all cases Z_1 is made a very high reactance.

The pattern of the electric field in the interaction space has been measured on cold test models by the use of an electrostatic probe on a rotating dummy cathode. Under proper conditions a pattern similar to that shown by the solid lines in Figure 4.8 is obtained. However, when $Z_1 \neq Z_2$, for the same total voltage across the teeth the field pattern will be modified to that shown by the dotted lines. It is seen that when $Z_1 \neq Z_2$ the field pattern is markedly asymmetrical.

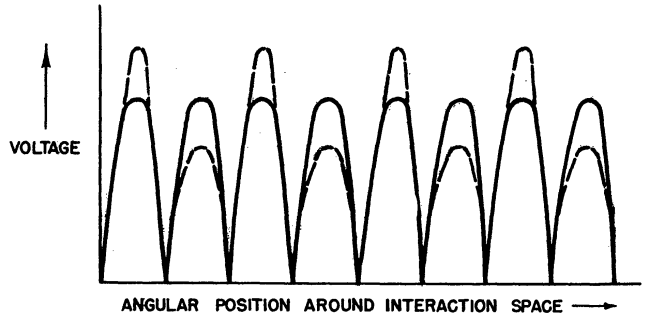

FIG. 4.9 ELECTRIC FIELD PATTERN IN INTERACTION SPACE.

5. EXPERIMENTAL INFORMATION ON HIGHER ORDER MODES

Two types of higher order modes have been observed in experimental measurements on models of interdigital magnetron cavities. One type, in which nodes in the electric field occur on circles between the inner and outer cavity boundaries, can be treated analytically by the theory of Section 3. For a given value of the tangent defined in Formula (3.3), a number of values of θ_c exist. These values of θ_c correspond to values of $\frac{2\pi R_c}{\lambda}$ for which nodes exist in radially standing waves on the radial transmission line. Several modes of this type have been studied experimentally. Calculated and observed values of R_c are tabulated in Table 5.1. R_c is used as a calculated quantity

because Formula (3.3) cannot be solved explicitly for λ. The probe used in the measurements could not be placed in close enough to the anode to locate the node which theoretically existed just outside R_a (at about 1.7 cm). However, a maximum reading was observed between the probe position located closest to the anode and the outer boundary of the cavity.

TABLE 5.1

Measurements on Model Interdigital Structure TM020 Mode

C_A Calculated $\mu\mu f$	λ obs. cm	h meas. cm	R_a meas. cm	R_c meas. cm	R_c calc. cm
4.2	9.6	2.54	1.59	6.68	6.5
4.2	11.44	2.54	1.59	7.63	7.7
4.2	11.9	2.54	1.59	7.93	8.0

The possibility of error if care is not exercised in the theoretical approach used is illustrated by the measurements in Table 5.2. In this case, the loading capacitance of interdigital anodes was replaced by a center post spaced close to one face of the cavity. The first set of measurements and calculations show good agreement where Formula (3.3) is used. For the second set the cavity boundary is placed at the node closer to the loading capacitance. In this case, Formula (3.3) does not give good agreement. However, if the cavity is considered as a coaxial transmission line rather than a radial transmission line, a better result is obtained. In this case the familiar formula

$$\frac{\lambda}{2\pi c C_A} = 60 \log \frac{R_c}{R_a} \tan \frac{2\pi h}{\lambda} \qquad (5.1)$$

is used. This result shows that the interlocking finger structure tends to encourage modes of the radial transmission line type for, in actual interdigital magnetron cavities of similar geometry except for the form of the

loading capacitance, the agreement is good using Formula (3.3). These data are given with performance results in Section 7.

TABLE 5.2

Measurements on Model Cavity with Capacitive Loading Center Post

Post Spacing from Cavity Face cm	Loading Capacitance (calc.) $\mu\mu f$	λ obs. cm	h meas. cm	R_a meas. cm	R_c meas. cm	R_c calc. cm	Mode	Formula Used
.685	1.4	10.87	2.54	1.90	7.93	8.0	TM020	3.3
.26	1.5	12.34	2.33	1.15	1.59	1.96	TM010	3.3
.26	1.5	12.34	2.33	1.15	1.59	1.55	TEM001	5.1

All of the higher order modes of the type just discussed, wherein nodes occur radially in the cavity, are of much shorter wavelength than the zero order mode for the same cavity (separated by a factor of the order of 3 or 4 to 1). The resonant wavelength in the other types of higher order modes are separated by much smaller ratios. The first order mode, for example (TM110), is separated usually by a factor of less than 1.5 to 1 from the zero order mode (TM010). In this case, nodes in the electric field occur on diameters of the cavity, thus superimposing a variation in potential around the anode structure on the already alternately plus and minus potentials of the teeth. The effect of this mode on design for zero order mode operation is important and will be discussed further in Section 6. Analytical treatment of these modes has not been carried out by this project, but the general method used for the zero order mode analysis can be used.

Several experimental measurements have been made showing effect of cavity diameter on higher order modes of this type with the same cavities used for the measurements in Figure 5.1. One circumferential node is present for these measurements in all cases. The mode number is indicated on the curves.

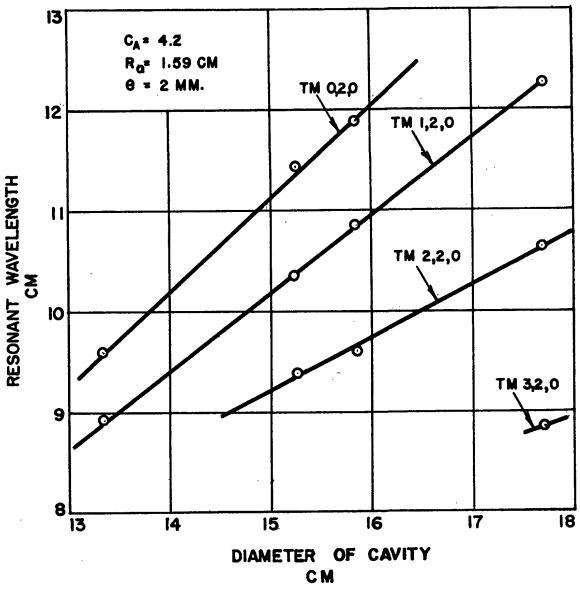

FIG. 5.1 EFFECT OF CAVITY DIAMETER ON RESONANT WAVELENGTH IN HIGHER ORDER MODES.

Anode spacing is the same in all cases. These data are interesting in that they show the increase in mode separation as outer cavity diameter is increased. This is more obvious in the data of Figure 3.6 which shows similar data on the fundamental and first order modes of a model structure which was more nearly similar to magnetrons actually built (approximately the same structure as the model 2 magnetron discussed in Section 7).

The major usefulness of these measurements was to indicate experimentally what other modes might be present and offer basis for an estimate of the effects of their presence on operation of the zero order mode. The most important modes, in that they are relatively near in resonant wavelength, are the first and second order modes. By these are meant the TM110 and the TM210. No extensive measurements have been obtained on these modes except on operating magnetrons. These are presented in Section 7. As the diameter of the cavity is decreased, it becomes difficult to make probe

measurements on actual size models of the magnetrons. Qualitative information has been obtained, however, with the aid of a rotating probe set in which the investigating probe is mounted on the dummy cathode. This technique has drawbacks in that the coupling to the cathode is unbalanced by the presence of the probe. For comparison, the 0, 1st and 2nd order modes, as they appear to exist from these tests, are sketched in Figure 5.2 with the anodes and interaction space shown. Operation in higher order modes, use of "buck teeth" to encourage the node, and problems of removal of the degenerate modes which exist at approximately the same wavelength when higher order modes are used have been studied in considerable detail by other laboratories.(1)

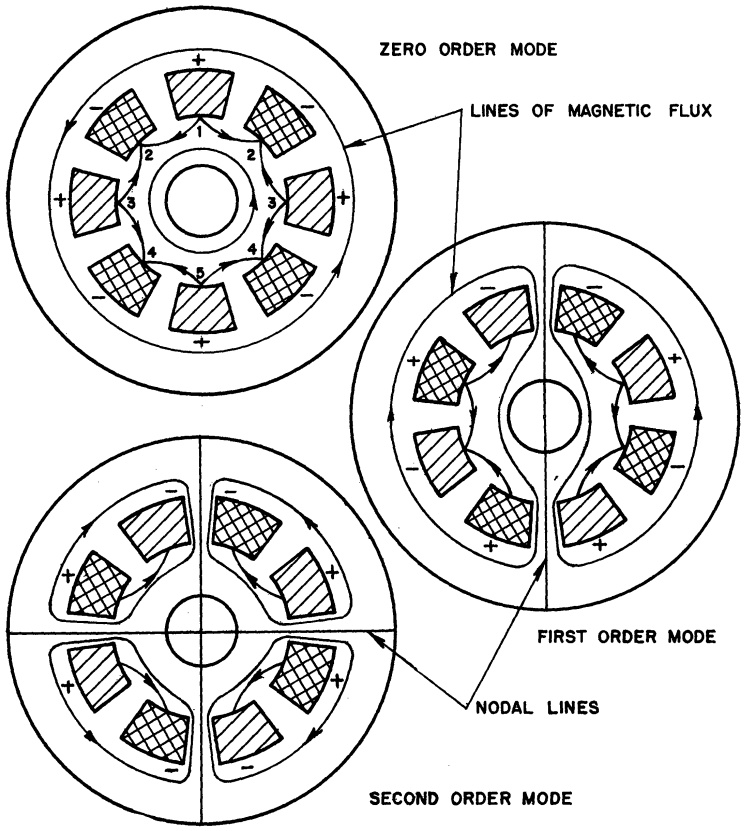

FIG. 5.2 CONFIGURATION OF 'E' AND 'H' FIELD LINES IN INTERACTION SPACE.

---

(1) Crawford, F. H. and Hare, M. D., "A Tunable Squirrel Cage Magnetron, The Donutron", Proc. IRE, Vol. 35, No. 4, pp. 361-369, April 1947.
"Obstacle-loaded Cylindrical Cavities with Application to the Interdigital Magnetron", Tech. Report No. 60, Cruft Laboratory, Harvard University, November 1948.

6. INTERACTION SPACE AND DESIGN CONSIDERATIONS

The design of interdigital magnetrons for operation in the zero order mode involves the same types of problems which exist in the vane magnetron. However, certain points are sufficiently unique to deserve special mention.

The interaction space design may be carried out on the basis of the dimensionless variables defined in Technical Report No. 1 of this laboratory. Quantities depending on the dimensions of the interaction space and the resonant wavelength are defined as follows:

$$E_o = \frac{m}{2e} \left(\frac{2\pi c}{n\lambda}\right)^2 r_a^2 \quad \text{volts} \tag{6.1}$$

$$B_o = \frac{2m}{e} \left(\frac{2\pi c}{n\lambda}\right) \frac{1}{1 - \frac{r_c^2}{r_a^2}} \quad \text{webers/meter}^2 \tag{6.2}$$

$\frac{e}{m}$ = specific charge of electron

n = mode number ($\frac{N}{2}$ for zero order mode, $\frac{N}{2} \pm 1$ for first order mode)

N = total number of anode segments

λ = wavelength of oscillation

r_c = cathode radius

r_a = anode radius

c = velocity of light

In terms of these quantities the Hartree voltage for initiation of oscillation is:

$$\frac{E}{E_o} = 2B/B_o - 1 \tag{6.3}$$

where

E = magnetron anode volts

B = magnetron magnetic field

The maximum possible electronic interaction efficiency, assuming the electrons reach the anode with the angular velocity of the electromagnetic wave, is given by

$$\eta_e = \frac{\frac{E}{E_o} - 1}{\frac{E}{E_o}} \tag{6.4}$$

Thus, for interaction efficiency greater than 80 per cent, E/E_o must be greater than 5. This places certain restrictions on r_a and n and determines B/B_o through Equation (6.3). Another design parameter developed by Allis and Slater which affects the operating current is sometimes used in magnetron design.

Slater defines

$$I_o = \frac{2\pi a_1}{\left[1 - \frac{r_c^2}{r_a^2}\right]^2 \left[\frac{r_a}{r_c} + 1\right]} \frac{m}{e} \left(\frac{2\pi c}{n\lambda}\right)^3 r_a^2 \epsilon_o L \text{ amperes} \tag{6.5}$$

Here

a_1 = approximately 1 in range of r_a/r_c between 1.3 and 3.5

ϵ_o = dielectric constant of free space

$= \frac{1}{36\pi} \times 10^{-9}$ farads/meter

L = length of emitting surface

In practice it is found that the current for which magnetrons stop oscillating is approximately defined by

$$\frac{I}{I_o} = \frac{1}{2} \left(\frac{E}{E_o}\right)^{3/2} \tag{6.6}$$

This value of current is approximately two-thirds of the Langmuir diode current for the magnetron. It is also found in practice that operation at small values of I/I_o, i.e., $I/I_o < 0.1$, is inclined to be inefficient.

The conditions just described can be met by various combinations of r_a, r_c, n, L and λ. However, other restrictions must be considered. λ,

of course, is defined by the objective for which the tube is being designed. The next most important limiting factor is the available cathode emission. This must be sufficient to supply the current for which the tube is to be rated, plus a suitable margin. It is desirable that at least three times the rated current is available in the cathode. Because of physical limitations and available emission densities, choice of r_c and L is limited by this fact.

These restrictions apply to any type of magnetron. Other special restrictions arise when the resonant circuit of the interdigital tube is considered in relation to the interaction space limitation.

It is desirable that the fingers of a high power interdigital structure be short and thick for purposes of heat dissipation. It is also desirable that the space between cathode end hats be less than the length of the fingers, minus the maximum end spacing experienced in tuning (ℓ - e, see Figure 3.2). This tends to prevent electrons being exposed to axial fields which cause leakage out the end spaces. The two restrictions just mentioned are conflicting and compromise must be reached in design. At the present state of the development in this laboratory, it is believed that no excessive difficulty should be experienced with the design of tubes capable of dissipating as much as a kilowatt of anode power. Examination of the assembly drawings given in the next section will show that anode structures can be made quite rugged. Radial thickness of the teeth is not limited by the above considerations, but is limited insofar as the anode capacitance is affected. This, of course, in turn affects the design of the rest of the resonant circuit.

The circuit efficiency of interdigital magnetrons operating in the zero order mode is inclined to be lower than some other types of magnetrons, but is not necessarily excessively low. The reason for this is that the

unloaded Q (Q_o) is lowered by the effect of the cathode line on the circuit. A typical value of unloaded Q is less than 500; this means that for greater than 80 per cent circuit efficiency loaded Q's (Q_L) less than 100 must be used. Circuit efficiency is defined by

$$\eta_c = \frac{Q_o - Q_L}{Q_o} \tag{6.7}$$

The overall efficiency to be expected under these conditions, and assuming that $E/E_o > 5$, is

$$\eta = \eta_e \eta_c > .80 \times .80 = 64\%$$

If efficiency does not meet this value, then it should be explainable on the basis of some factor not taken into account. Typical calculations are given in the next section which will bear out this point.

One other factor which is of great importance in design is still not completely understood. This is the condition of optimum shunt impedance. The shunt impedance of an ordinary resonant circuit may be defined by:

$$Z_{sh} = \frac{Q_L}{\omega C} \tag{6.8}$$

Q_L = loaded Q

C = circuit capacitance into which electronic generator induces current

ω = angular frequency of oscillation

The quantity defined by Equation (6.8) is a definite determinable property of the circuit. In microwave circuits some ambiguity may exist because reactance is distributed rather than lumped. This is not usually serious, especially in the case of the interdigital magnetron. However, the relationship which the shunt impedance bears to electronic properties of the magnetron is not at all clear. No method, except experience with similar magnetrons, has been proposed for absolutely predetermining the optimum value of

shunt impedance for a given interaction space design. The following represents briefly the type of analysis usually given.

If the shunt impedance is too high, efficiency tends to decrease. This is believed to be related to over-bunching caused by high r-f voltage. However, this condition does not occur in interdigital magnetrons operating in the zero order mode because Q_L, as mentioned above, is necessarily low for good circuit efficiency and C tends to be high for increased anode dissipation. It is also believed that if shunt impedance is too low, low efficiency results because low r-f voltage encourages de-bunching and leakage. For higher circuit efficiency, however, Q_L should be low and this effect is probably more important in the design of interdigital tubes.

The problem of mode jump introduces other restrictions. Mode jump current seems to be affected by at least three factors: shunt impedance, presence of other modes, and cathode emission. It is not the current defined by Equation (6.6), for which oscillation ceases. Low shunt impedance seems to cause low mode jump current if another mode is present in which conditions are more favorable for oscillation. Thus, to raise mode jump current in a given magnetron, one would expect to do one or more of the following: increase Q_L, decrease C, increase mode separation. The first and second of these steps tend to conflict with conditions for optimum efficiency and the second step conflicts with maximum heat dissipation requirements. Anodes of the type shown in Figure 3.8 are helpful in reducing this dilemma. More heat is conducted through the base of the anode finger than through the center or the tip so that tapered teeth will reduce capacitance without seriously affecting heat dissipation capability.

The relation of various factors which affect mode separation is not clearly defined, but experience with tubes built in this laboratory

seems to be consistent with qualitative predictions. Pertinent data on these tubes are given in Table 6.1. An increase in outer cavity radius causes greater increase in wavelength of the zero order mode than the first order mode. This is a result of a greater concentration of magnetic field in the first order mode in the vicinity of the teeth. For the same reason, a decrease in inner cavity radius should cause a greater decrease in the resonant wavelength of the first order mode than in the resonant wavelength zero order mode. The effective voltage between teeth in the first order mode is less because of the superimposed voltage distribution around the anode. Capacitance changes might be expected, therefore, to have greater effect on the zero order mode. In Figure 6.1 the percentage mode separation is plotted against $\sqrt{C_A}\ R_c/\frac{R_a + r_a}{2}$ for four tube models built in the Michigan laboratory. The mean anode radius $\frac{R_a + r_a}{2}$ is used because in all of the tubes except model 4 the fingers have relatively large radial thickness. Wavelength is proportional to $\sqrt{C_A}$ which accounts for the use of this factor.

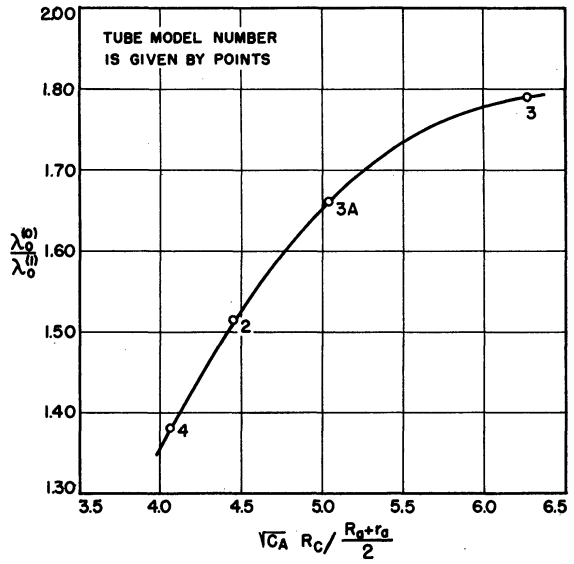

FIG. 6.1 EFFECT OF RESONANT CIRCUIT PARAMETERS ON MODE SEPARATION

TABLE 6.1

Factors Affecting Mode Separation

Magnetron Model No.	C_A $\mu\mu f$	Mean Anode Radius $\frac{R_a + r_a}{2}$ cm.	Cavity Radius R_c cm.	$\lambda_o(0)$ Zero Order Meas. cm.	$\lambda_o(1)$ First Order Meas. cm.	$\frac{\lambda_o(0)}{\lambda_o(1)}$	$\sqrt{C_A \frac{R_c}{\frac{R_a + r_a}{2}}}$
2	3.35	.910	2.22	15.6	10.2	1.53	4.45
3	4.96	.675	1.90	17.0	9.5	1.79	6.26
3A	4.96	.675	1.52	14.6	8.8	1.66	5.03
4	4.52	.895	1.71	14.6	10.6	1.38	4.06

The role of cathode emission in determining mode jump current is possibly related to the same factors which underly the empirical Formula (6.6). Tubes using thoriated tungsten cathodes experience a radical reduction in mode jump current when temperature limited current is reduced by deactivation of the thoriated tungsten. Some observations have been made in this laboratory on tubes with tungsten cathodes which definitely show that increasing cathode temperature increases mode jump current in all modes. In the highest voltage mode, the mode jump occurs at approximately the value of current given by Equation (6.6), but for lower voltages the mode jump current is less.

It is advisable to separate as much as possible in voltage the zero and first order modes in order to eliminate the possibility of preferential operation in the first order mode at the voltage to be used for the zero order mode. If the ratio $\frac{\lambda_o^{(0)}}{\lambda_o^{(1)}}$ is known this separation can be readily calculated. Re-writing Equation (6.3) for the voltage at which oscillation is initiated

$$E = \frac{E_o}{B_o}(2B - B_o) \tag{6.9}$$

Let the superscript (0) indicate values for the zero order mode and the superscript (1) values for the first order mode. Then, using Equations (6.1) and (6.2)

$$\frac{E^{(1)}}{E^{(0)}} = \frac{E_o^{(1)}/B_o^{(1)}}{E_o^{(0)}/B_o^{(0)}} \frac{(2B - B_o^{(1)})}{(2B - B_o^{(2)})} \tag{6.10}$$

$$\simeq \frac{N/2}{N/2 + 1} \frac{\lambda_o^{(0)}}{\lambda_o^{(1)}}$$

This last approximation is valid if E/E_o is large, as it should be for efficient operation. This result is rather interesting because it means that N should be large for good voltage separation. In the ordinary system of Hartree

harmonics, the nearest mode is the N/2 - 1 mode, which means that N should be small for good voltage separation. The N/2 + 1 mode is introduced by the superimposed voltage distribution in the first order mode.(1)

Good voltage separation is to be expected, therefore, if the number of anodes and the wavelength ratio are kept large. The anode capacitance is proportional to N/r_a since spacing between teeth is usually made $\frac{2\pi r_a}{2N}$. Thus large N and small r_a tend to result in a large value for C_A. These factors all appear to be desirable for good voltage separation as well as high efficiency, so therefore should indicate the direction to be taken in future design.

7. TUBE PERFORMANCE

The major purpose of this section is not to give all the details of construction and performance on each of the tubes built in the Michigan Laboratory, but to point out by examples the validity of the general principles of design which have been set forth. Three basically different models have been designed and operated, the model 2, model 3 and model 4 magnetrons. The model 3A is different from the model 3 only in the cavity diameter. The model 4A' is different only in cathode choke design from model 4. Neither model 4 nor model 4A will operate in the zero order mode. A second revision which it is hoped will correct this is under construction at the present time. Assembly drawings of all the tubes are given in the appendix. An exploded view of the parts for one of the tubes is shown in Figure 7.1. Details of construction will be described in the final report of this project

---

(1) See Chapter 22 of "Very High Frequency Techniques", Radio Research Laboratory Staff, McGraw-Hill, New York and London 1947.

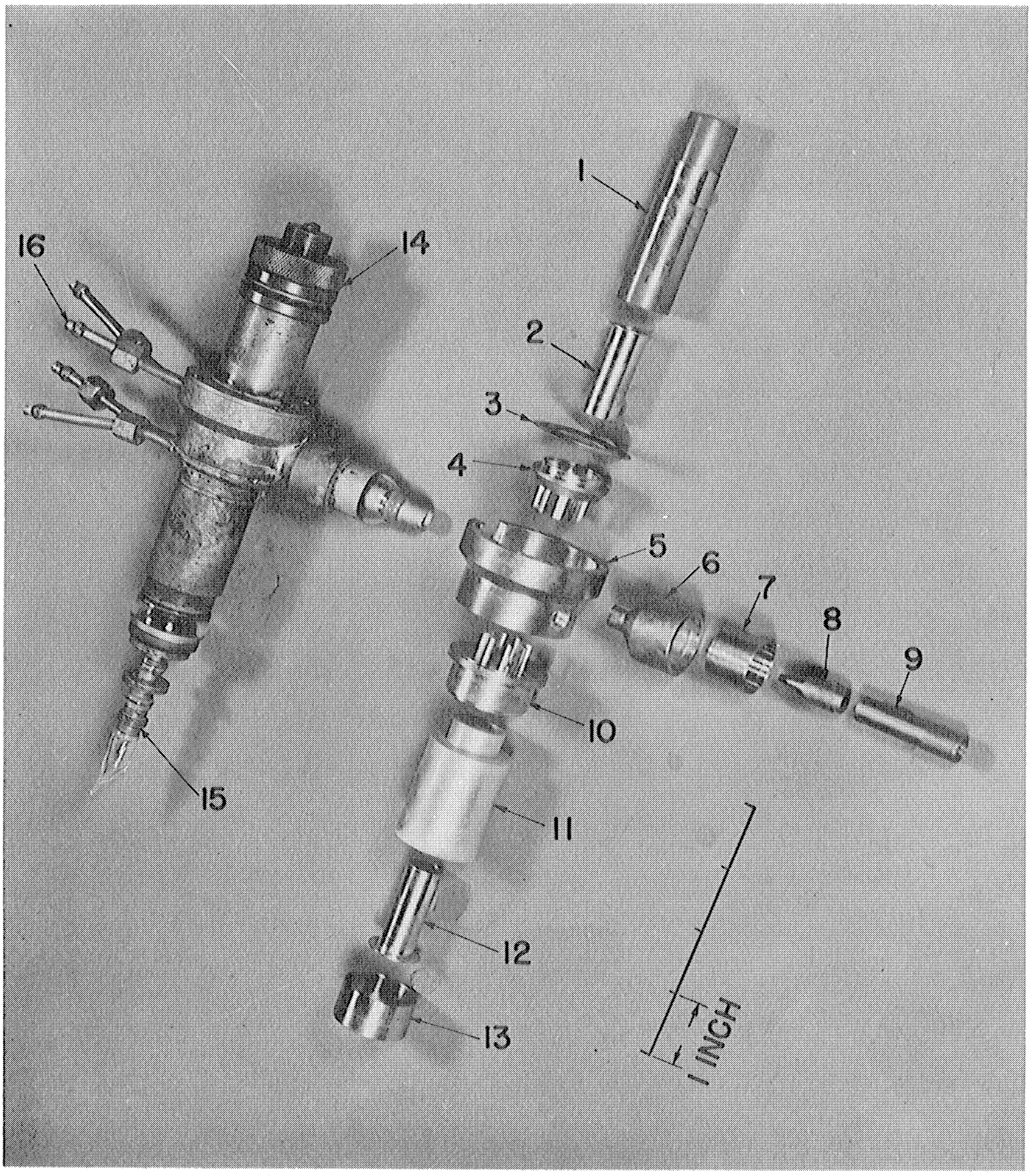

Figure 7.1 Interdigital Magnetron and Parts

1. Tuner screw
2. Tuner choke
3. Diaphragm
4. Diaphragm anode
5. Cavity
6. Outside taper
7. Outside Kovar
8. Inside taper
9. Inside Kovar
10. Cavity anode
11. Cathode pole piece
12. Cathode choke
13. Kovar sleeve
14. Tuner pole piece assembly
15. Cathode assembly
16. Water cooling tubes

TABLE 7.1

Design Parameters Used in Magnetrons Constructed at University of Michigan

Magnetron	r_a cm	r_c cm	$\frac{r_a}{r_c}$	L cm	R_a cm	R_c cm	h cm	ℓ cm	d cm	N	C_A $\mu\mu f$	λ cm	E_c volts	B_o gauss	E volts	B gauss
Model 2	.665	.27	2.46	.660	1.18	2.22	1.54	1.27	.259	8	3.35	15	1230	376	5000	1000
Model 3	.45	.27	1.66	.660	.900	1.90	.95	.834	.117	12	4.96	16	220	349	2500	2000
Model 3A	.45	.27	1.66	.660	.900	1.52	.95	.834	.117	12	4.96	13	335	430	2500	2000
Model 4	.665	.381	1.75	.300	.925	1.71	1.03	.875	.130	16	4.52	14	355	286	2500	900

TABLE 7.2

Summary of Performance of Magnetrons Built at University of Michigan

Magnetron	λ_o (cm)		Mode	E_o	B_o	E	B	B/B_o	$\frac{E_{Hartree}}{E_o}$		Q_o	Q_L	η_e(%) calc.	η_c(%)	η(%) calc.	
	calc.	meas.		volts	gauss	volts	gauss		calc.	meas.	meas.	meas.	max.	calc.	max.	meas.
Model 2	15	15.6	$n=\frac{N}{2}=4$	1130	360	4400	900	2.5	4.0	3.9	503	251	75	48	36	22.5
Model 3	16	17.0	$n=\frac{N}{2}=6$	196	329	2500	2100	6.4	11.8	12.7	510	120	92	76	70	72
Model 3A	13	14.6	$n=\frac{N}{2}=6$	266	383	2400	2100	5.5	9.0	9.4	--	--	89	55 est.	48 est.	43 at 15.8 cm
Model 4	14	14.6	$n=\frac{N}{2}=8$	327	274	2100 calc.	1000 assumed	3.7	6.4	--	98	58	84.5	41	34	--

(Technical Report No. 3). In all, 18 tubes have been started in construction. Three of these were lost in early stages of construction; six were lost during the evacuation process; two were lost after completion and before tests were made; seven were operated in experimental tests. Three of these tubes are still operable. One of these has been tipped off for almost a year and a half. The tubes which have been operated consist of the following: two model 2's, two model 3's, one model 3A, one model 4 and one model 4A. All tubes have diaphragm tuning.

The parameters used in design are tabulated in Table 7.1. The first tubes, models 2, 3 and 3A, were constructed to use a thoriated tungsten cathode purchased from Litton Engineering Laboratories. The model 4 uses a tungsten cathode constructed in this laboratory. The anode capacitance and outer cavity radius are calculated using formulas (3.11) and (3.3) with Figure 3.3. Other considerations used in design were based on the desirability of having available a number of differently constructed magnetrons for experimental study. Thus, the model 2 is not expected to be efficient in low voltage operation, but it is expected to be useful in studies of behavior of magnetron space charge and analysis of interdigital magnetron performance.

A comparison of results with theoretically predicted performance is given in Table 7.2. These results all correspond to anode end spacing equal to the spacing between adjacent teeth for the reason that this condition is used for calculation of capacitance and resonant wavelength.

The measured resonant wavelength is always higher than the calculated value. Agreement is best for the model 2 and model 4 magnetrons and worst for the model 3. The fact that the wavelength always measures longer

is probably due to underestimation of the anode capacitance. The effects of the cathode and the choke structure could easily account for 6 to 8 per cent error in capacitance and therefore 3 to 4 per cent error in wavelength. The geometry of the model 3 magnetron cavity is possibly not simple enough to justify use of the simplified approach of Section 3. Examination of the assembly drawing of this tube will show that the thickness of the teeth is almost half the radial cavity thickness ($R_c - r_a$). Thus, consideration of the capacitance as lumped at R_a is not an accurate assumption. Some smaller radius, which would give a longer calculated wavelength, should probably be chosen.

The agreement in the Hartree voltages is relatively good, although no particular attempt has been made to check these with great accuracy. Data are not available on model 4 since it does not operate in the zero order mode.

Circuit efficiency is calculated on the basis of measured values of Q. The electronic efficiency is calculated from E/E_o by the method outlined in Section 6. The maximum over-all plate efficiency is calculated as the product of electronic and circuit efficiency. Agreement is good in the case of model 3, as is usually found to be the case in tubes having high efficiencies. In the case of model 2 the measured efficiency is low compared to the calculated. In cases where the anode current used in an efficiency measurement is near the mode boundary low efficiencies are usually observed. This is probably related to the effects of poor bunching mentioned in the last section. Operation at higher voltage was attempted on this tube, but both efficiency and mode jump current were affected adversely. This would indicate that shunt impedance is low in the model 2. However, any steps taken to increase shunt impedance would decrease circuit efficiency, which is already low.

The only Q measurements available on the model 3A were made without the presence of the cathode. The result of these measurements was $Q_o = 790$, $Q_L = 89$. This tube was inoperable over half the tuning range because the design of the choke and by-pass combination was not changed to conform to the change in cavity diameter. However, estimating a circuit efficiency of about 55 per cent (this is in line since Q_o would be lowered by the power coupled out the cathode line) the over-all efficiency can be estimated at less than 50 per cent. The highest measured efficiency at 15.8 cm is 43 per cent.

The low Q_o and low calculated efficiency on model 4 illustrate the importance of having properly designed choke and by-pass combination in the cathode line. The distance from choke short to anode base in this tube is .26λ at 14.6 cm. This was not felt to be sufficiently different from .25λ to cause trouble when the tube was designed, especially in view of the fact that at one point in the tuning range the length is .25λ (15.2 cm). However, the by-pass spacing was made large to allow for passage of the end hats upon insertion of the cathode and the over-all effect was to have very strong coupling to the cathode line. A number of Q measurements have been made on a model of this tube with various changes in exact geometry of the cathode circuit. These are given in Table 7.3. They serve to illustrate that it is important that certain of the details of geometry be duplicated in the model when making such measurements. The presence of the kovar cup to which the cathode seal is made, for instance, reduces the unloaded Q by a factor of nearly 1/2 in the model 4 structure. The over-all experience indicates that the exact method for locating cathode chokes outlined in Section 4 should be used and that the by-pass should be spaced as close to the cathode as possible. Model 4 is being redesigned on the basis of these results.

TABLE 7.3

Q Measurements on Brass Model of Model 4A Magnetron at 14.5 cm

	Conditions of Test	Measured Q_o
1	No cathode	804
2	Brass cathode By-pass shorted	494
3	CRS and Kovar cathode (to duplicate surface resistance properties of cathode) By-pass shorted	312
4	Same as 3, by-pass duplicating model 4A design	134
5	Actual cathode from Model 4A tube	140
6	Same as 3, by-pass built with close spacing	362
7	Same as 6, axial position of by-pass adjusted for optimum Q	480
*8	Model 4, serial No. 18 Same anode spacing as above data	98
9	Model 4, first order mode at 10.6 cm	3070

* It was found that this reading could be affected by metal in the vicinity of the cathode or by applying heater power; in the latter case Q_o is reduced to immeasurable values.

Performance of the model 2, model 3 and model 3A magnetrons is summarized graphically in Figures 7.2 and 7.3. Models 3 and 3A are covered by the same graph since the only difference in these models is the cavity diameter. The relative lengths of the choke and by-pass combination are plotted with the efficiency and mode jump curves to show that optimum

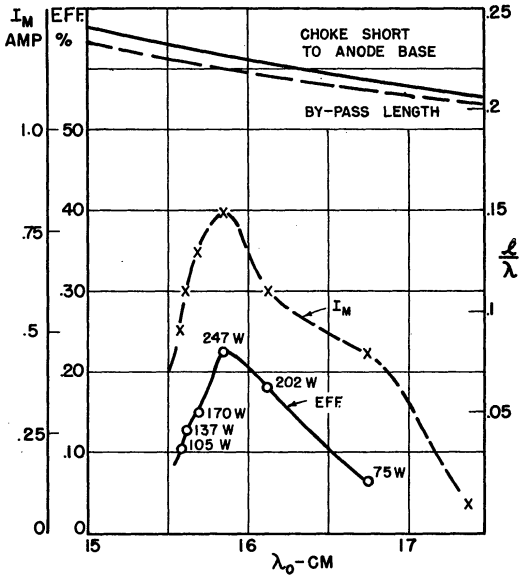

FIG. 7.2 CHART SHOWING EFFICIENCIES, I_M (=MODE CURRENT) CATHODE BY-PASS SLEEVE LENGTH AND DISTANCE FROM ANODE BASE TO CATHODE CHOKE SHORT IN MODEL 2. $E_b \cong 4500$ VOLTS $I_b = .25$ AMP

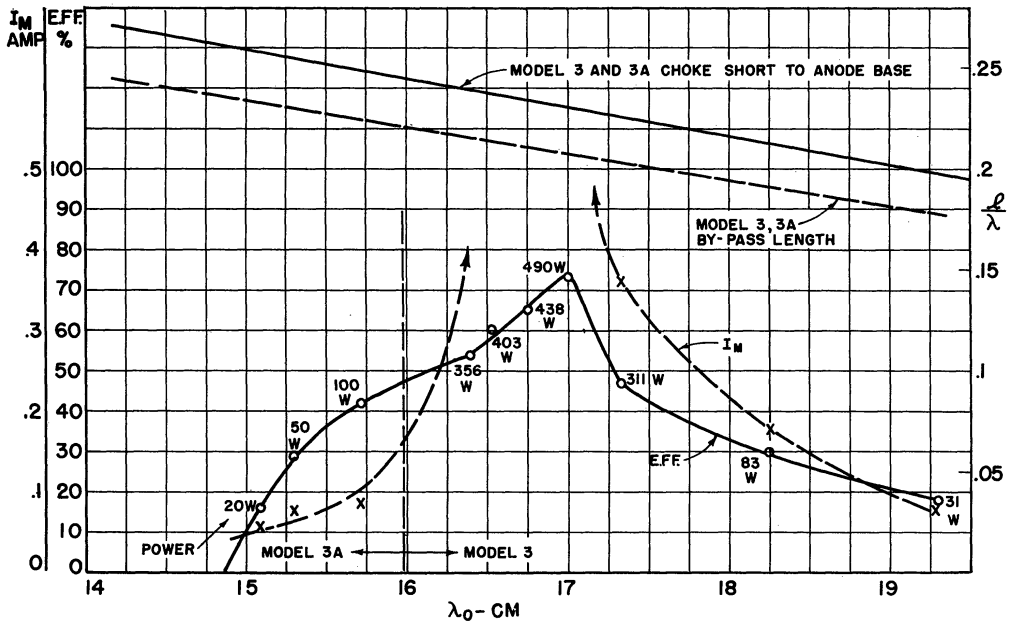

FIG. 7.3 CHART SHOWING EFFICIENCIES, I_M (= MODE CURRENT) CATHODE BY-PASS SLEEVE LENGTH AND DISTANCE FROM ANODE BASE TO CATHODE CHOKE SHORT IN MODELS 3 AND 3A. $E_b = 2200$ VOLTS $I_b \cong .3$ AMP FROM 16 TO 18 CM

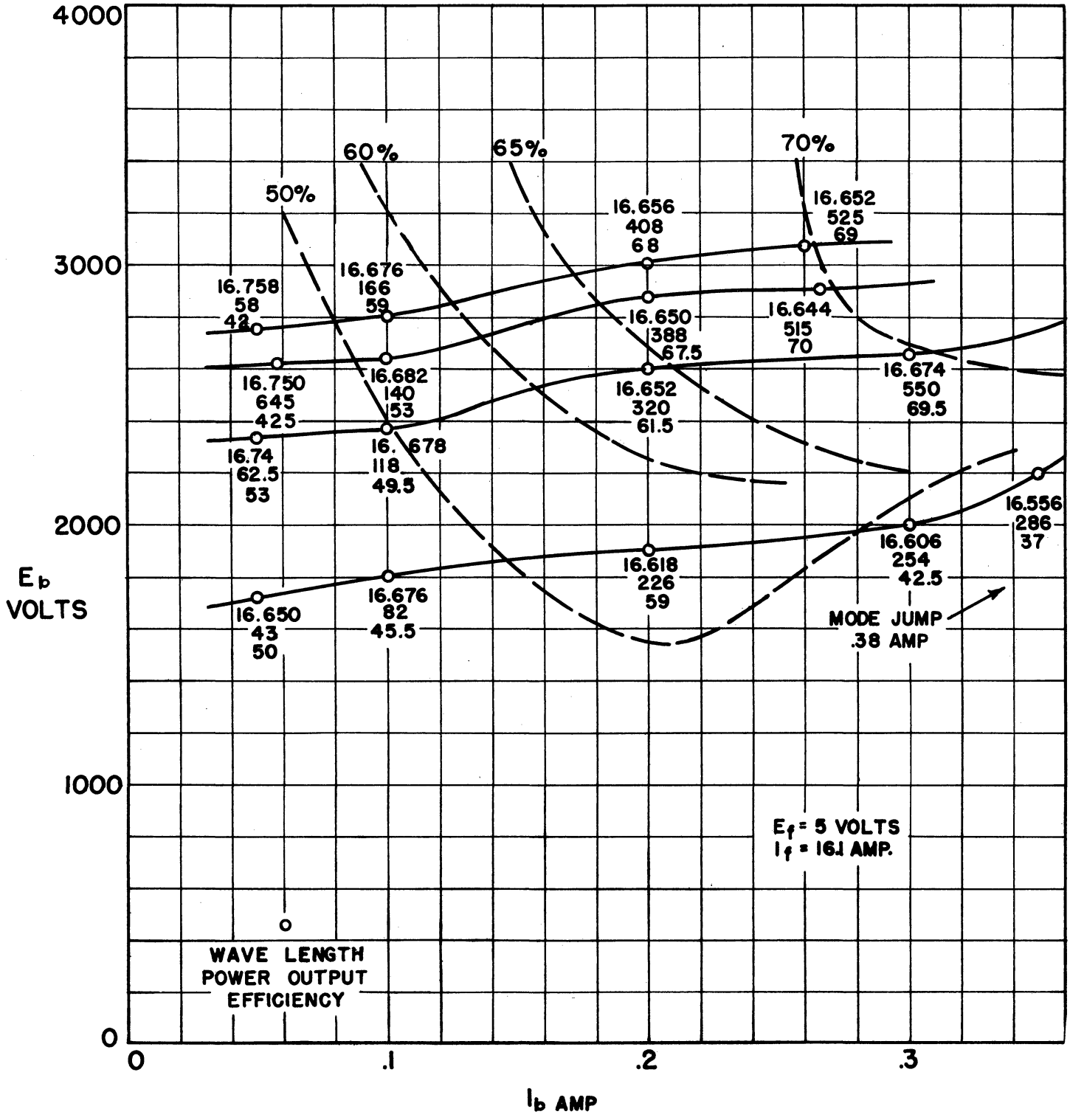

FIG. 7.4 PERFORMANCE DATA

MAGNETRON SERIAL NO. 8 MODEL 3
ZERO ORDER MODE
ANODE SPACING .052 INCHES
MATCHED LOAD

TABLE 7.4

SUMMARY OF MEASUREMENTS ON HIGHER ORDER MODES, MODEL 3 AND MODEL 4

Magnetron	λ_o(meas)	Mode Number	Mode Order	E_o	B_o	E/E_o	B/B_o	E_{cutoff} (Hull)	calc.	$E_{Hartree}$ obs. (approx)
	cm			volts	gauss			volts	volts	volts
3	17	$n=\frac{N}{2}=6$	0	196	329	5.07	3.04	1800	995	1000
3	9.5	$n=\frac{N}{2}+1=7$	1	460	504	2.98	1.97	1800	1370	1500
3	9.5	$n=\frac{N}{2}-1=5$	1	900	705	1.86	1.44	1800	1680	2100
4	15	$n=\frac{N}{2}=8$	0	310	266	6.5	3.76	4400	2010	--
4	11	$n=\frac{N}{2}+1=9$	1	454	322	5.2	3.1	4400	2360	2300
4	11	$n=\frac{N}{2}-1=7$	1	750	414	3.84	2.42	4400	2880	2700
4	7.5	$n=\frac{N}{2}+2=10$	2	790	425	3.7	2.36	4400	2920	2900

efficiency does not occur at .25λ for either choke or by-pass length. Volt-ampere characteristics for model 3 are shown in Figure 7.4. The usable tuning range is indicated by the efficiency curves. Typical tuning curves were given in Section 3 (Figure 3.7) for the zero and first order modes in model 4.

Measurements on the higher order modes are summarized in Table 7.4 for the model 3 and model 4 magnetrons. The Hartree voltages were taken from an oscilloscope screen and are approximate. Efficiencies were not measured in these modes because in all cases it is low. The unloaded Q is usually very high in higher order modes (see measurement No. 9, Table 7.3) and coupling is not strong. E/E_0 is low for the magnetic fields used. Thus, unless the magnetron is especially designed for higher order mode operation average circuit efficiency and low electronic efficiency, therefore, low over-all efficiency is to be expected.

8. POSSIBLE ALTERNATIVE STRUCTURES

Although the toroidal cavity loaded with interlocking fingers at the center is the type of resonant circuit employed in the interdigital magnetrons built in this laboratory, several other structures can be proposed. These have some similar characteristics and advantages to the toroidal cavity.

1. Coaxial Transmission Line Cavity Loaded with Modified Finger Structure[1]

Figure 8.1 shows a representative type of structure involving a coaxial line as part of the resonant element. The line of Figure 8.1 is λ/2 long, loaded with the capacitance of the vane structure at the center (high voltage point). Tuning can be accomplished by means of movable plungers replacing the end walls, or by any of several other methods. Structures of

(1) This structure was proposed by Mr. Gunnar Hok.

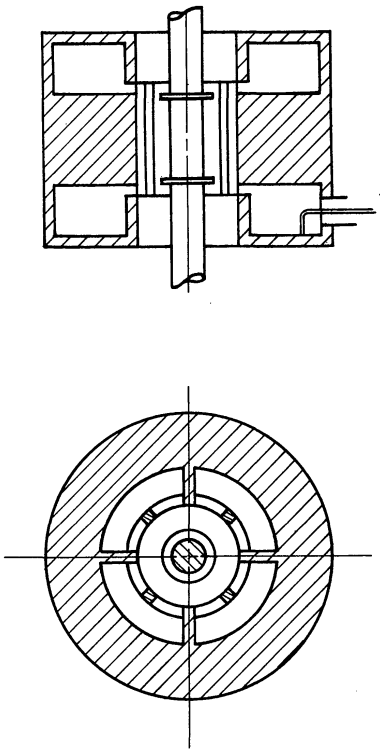

FIG. 8.1 PROPOSED COAXIAL MAGNETRON ANODE STRUCTURE.

this type with two sets of anodes lend themselves to frequency modulation by means of space charge clouds.

Brass models of a tube similar to that represented in Figure 8.1 have been built and tested. They were found to have the properties predicted by theory as far as wavelength, tuning, etc. One important factor in the design of such a tube to result from these investigations is the requirement that the ratio of inner to outer conductor diameters must be large. This is necessary in order to maintain the length of the vanes short enough that the resonant wavelength of the "vane mode" is reduced to far below the wavelength of the cavity or desired mode. By vane mode is meant the field configuration in which the vanes themselves and the sectors between vanes can form a resonant circuit; this is identical with the resonance in a vane type magnetron.

An f-m magnetron with two anode sets has been constructed employing these general principles and oscillations were obtained at the predicted wavelength.

2. "Push-pull" Type of Structure

An interdigital magnetron structure, involving the placement of two sets of interlocking teeth in a rectangular cavity, is shown in Figure 8.2. The desired mode in this structure involves a field pattern with maxima at each set of anodes so that the cavity will be electrically one wavelength long.

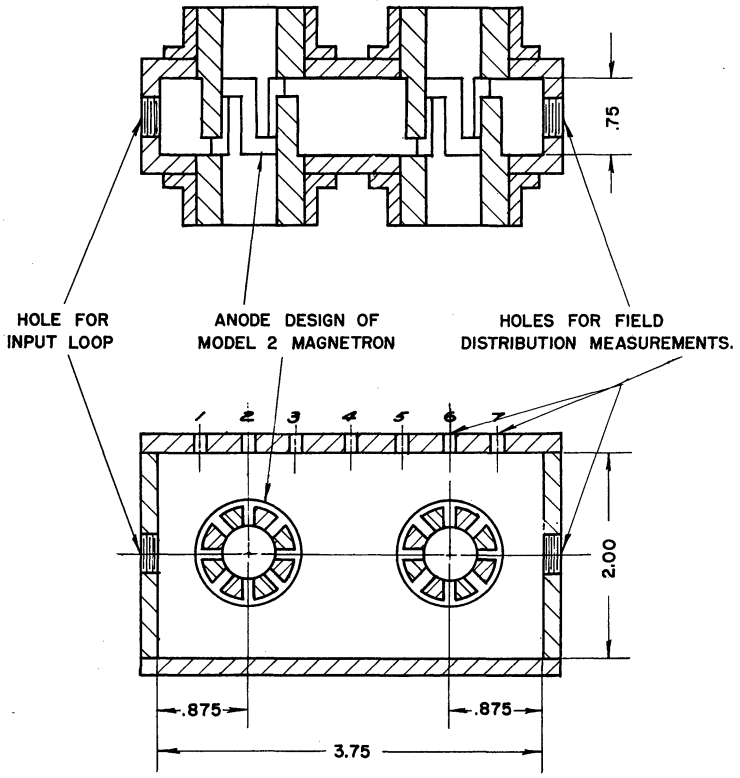

FIG. 8.2 RECTANGULAR CAVITY MAGNETRON
DIMENSIONS IN INCHES

A model of this structure was constructed of the dimensions shown in Figure 8.2 and measurements made of the magnitude of the magnetic field at various positions along its length. The results of measurements in the cavity alone, without finger anodes, are shown in the curves of Figure 8.3. It is seen that the relative field strength, being proportional to the square root of the probe reading, is symmetrical as expected. Both the full-wavelength and half-wavelength resonances are shown.

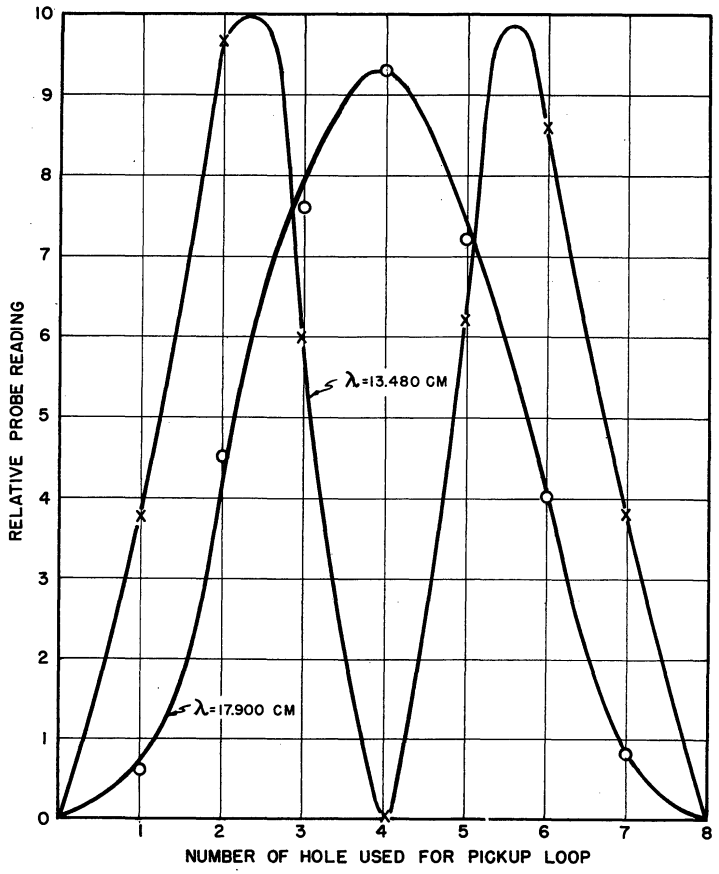

FIG. 8.3
FIRST AND SECOND ORDER MAJOR CAVITY RESONANCES IN RECTANGULAR CAVITY MAGNETRON. ANODES NOT IN PLACE

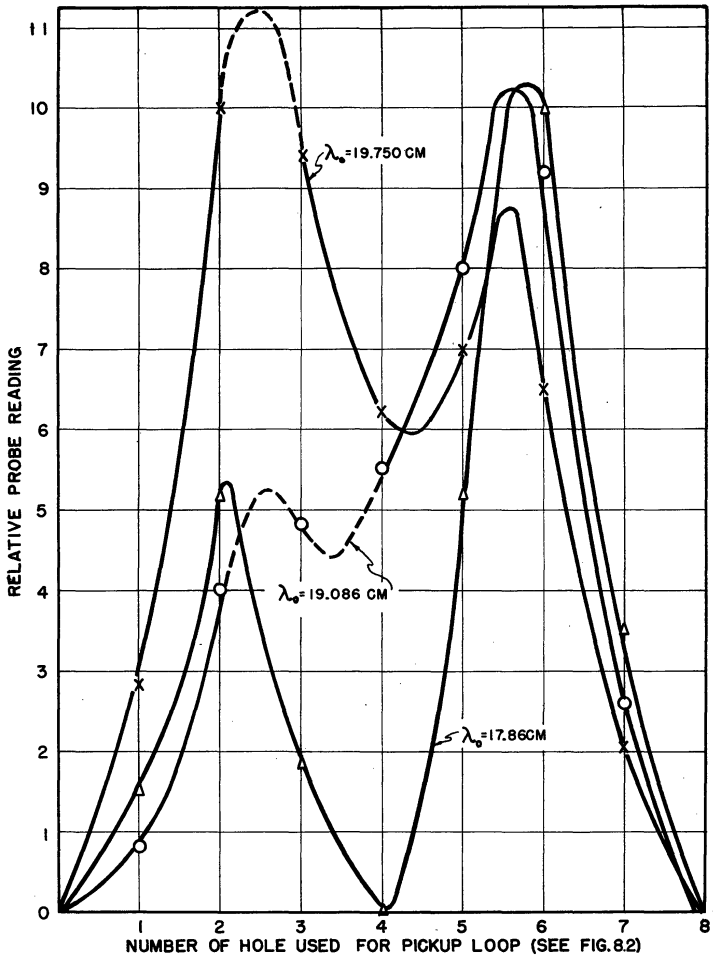

FIG. 8.4
RESONANCES FOR WHICH MAXIMA ARE LOCATED AT ANODE POSITION. CAVITY OF FIG. 8.2 ANODES IN PLACE

Upon insertion of the finger anodes a number of resonances were located, the principal ones as represented by the field pattern curves of Figure 8.4. It is seen that the pattern of the one-wavelength mode in Figure 8.3 is distorted to those shown in Figure 8.4, but is still clearly recognizable.

Except for the rather well-filled cold resonance mode spectrum, the preliminary measurements on this structure are encouraging. Possible applications may include frequency modulation by a space charge cloud in one set of anodes, or use as a high power source in which both anodes are used for oscillation, yielding a sort of push-pull effect. It can also be suggested that a number of such finger anodes could be arranged around a resonant transmission line formed into a closed circle, thus producing a magnetron source of very considerable power capabilities.

3. Coaxial Transmission Line with Interlocking Fingers

A modification of the interdigital magnetron, in which the inductance portion of the resonant circuit is provided by a coaxial line instead of the usual toroidal cavity, is shown in Figure 8.5. This line can be made electrically $\lambda/4$ or $3\lambda/4$ long loaded with the interlocking tooth structure on one end.

A tube of this type can be made widely and easily tunable and can be so constructed as to lend itself to frequency modulation by space charge clouds. Possible applications include use as a signal generator which would have the advantage of wide tunability.

A glass envelope interdigital anode is being used in a cavity of this type in the University of Illinois Tube Laboratory.

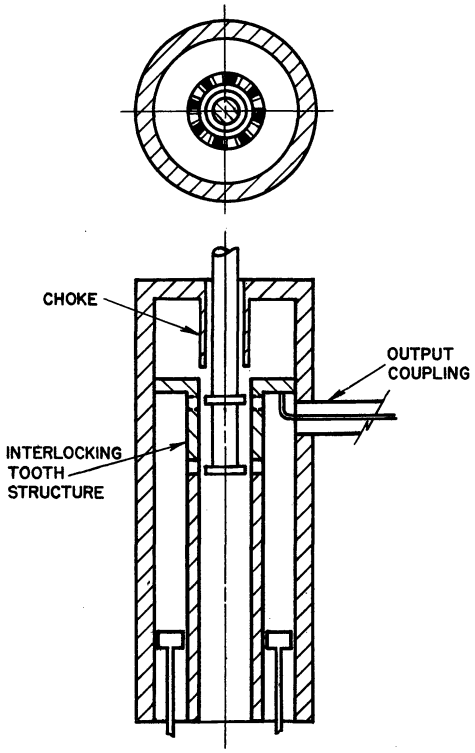

FIG. 8.5 PROPOSED COAXIAL INTERDIGITAL MAGNETRON.

9. CONCLUSIONS

The interdigital magnetron has been shown to be capable of high efficiency operation in the zero order mode. It is simpler in construction than other magnetrons usable in the same frequency range. On the basis of experience with three very differently designed structures, the agreement of results with theoretically predicted performance can be said to be good. The possibility of developing the interdigital magnetron for use in high power applications should therefore be given more serious consideration.

The wavelength range over which existing choke and by-pass combinations will function effectively is indicated by the theory and by the experimental results. The tuning range obtained by varying anode spacing is

greater than this, but so far no particular effort has been made to obtain a broad band design for the choke and by-pass. A better method of tuning probably exists, but this has also not been a subject for development by the project. The major purpose for the construction of these tubes was to test principles of design over a wide range of possibilities and gather information which would be useful in the development of a frequency modulation magnetron based on the interdigital type of structure.

A model 4 magnetron with an improved by-pass design will be built, but it is possible that due to small mode separation the tube will still not operate efficiently. If this is the case, improvements will be made along the lines of the model 3 which may hold more promise. Future efforts will be directed toward making broader band choke and by-pass combinations and obtaining tuning and frequency modulation. Any information which may give better understanding of magnetron operation, such as factors affecting mode jump current, etc., will of course be evaluated and studied as thoroughly as possible.

APPENDIX

Assembly Drawings of Interdigital Magnetrons Constructed at University of Michigan

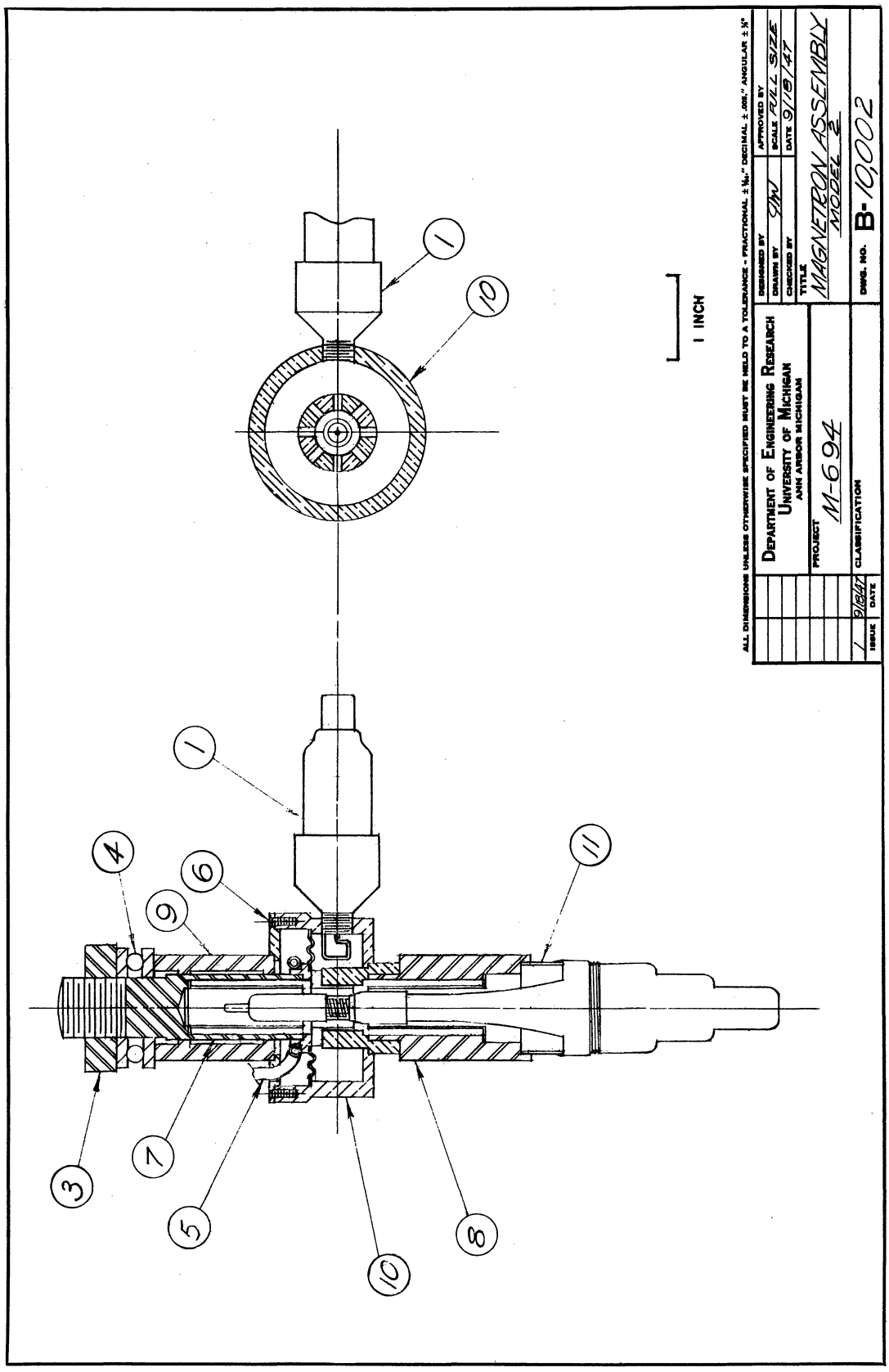
1
10
1 INCH
1
4
6
9
11
3
7
5
10
8
ALL DIMENSIONS UNLESS OTHERWISE SPECIFIED MUST BE HELD TO A TOLERANCE - FRACTIONAL ± 1/64" DECIMAL ± .005" ANGULAR ± 1°
DESIGNED BY
APPROVED BY
DEPARTMENT OF ENGINEERING RESEARCH
UNIVERSITY OF MICHIGAN
ANN ARBOR MICHIGAN
DRAWN BY DWJ
SCALE FULL SIZE
CHECKED BY
DATE 9/18/47
TITLE
MAGNETRON ASSEMBLY
MODEL 2
PROJECT
M-694
DWG. NO. B-10,002
ISSUE 1
DATE 9/18/47
CLASSIFICATION

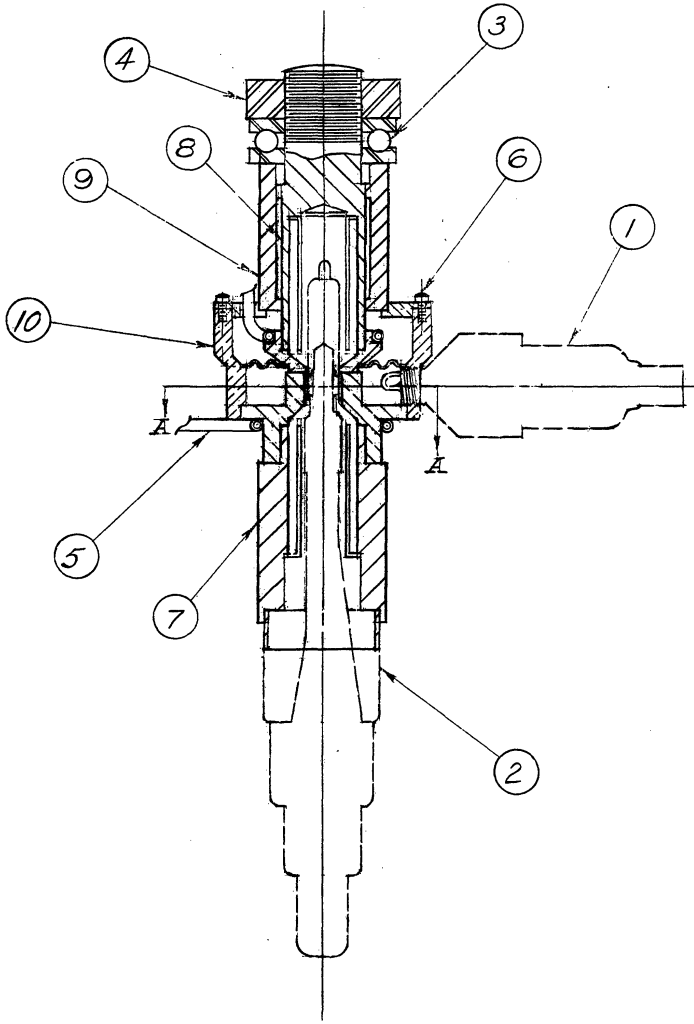

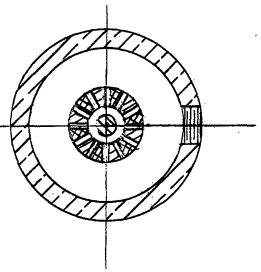

SECTION A-A

1 INCH

ALL DIMENSIONS UNLESS OTHERWISE SPECIFIED MUST BE HELD TO A TOLERANCE - FRACTIONAL ± 1/64" DECIMAL ± .005" ANGULAR ± ½°

		DEPARTMENT OF ENGINEERING RESEARCH UNIVERSITY OF MICHIGAN ANN ARBOR MICHIGAN	DESIGNED BY AWW, RSB	APPROVED BY AWW
			DRAWN BY JM	SCALE FULL SIZE
			CHECKED BY AWW	DATE 5/9/47
		PROJECT M-694	TITLE MAGNETRON ASSEMBLY MODEL 3	
1	5/9/47	CLASSIFICATION	DWG. NO. B-10,003	
ISSUE	DATE			

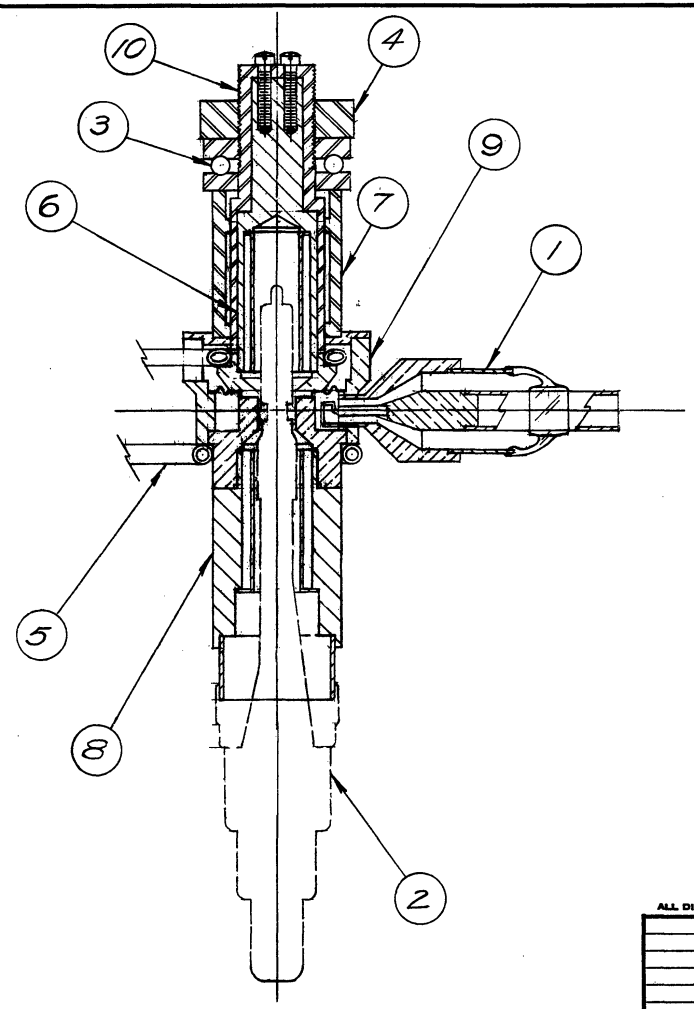

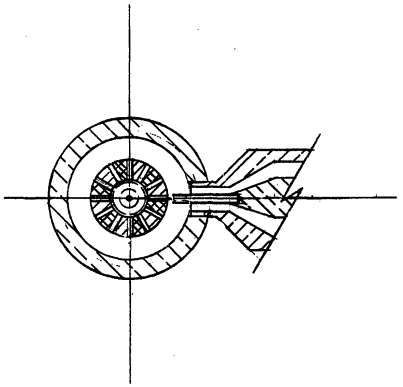

1 INCH

ALL DIMENSIONS UNLESS OTHERWISE SPECIFIED MUST BE HELD TO A TOLERANCE - FRACTIONAL ± 1/64" DECIMAL ± .005" ANGULAR ± 1/2°

		DEPARTMENT OF ENGINEERING RESEARCH UNIVERSITY OF MICHIGAN ANN ARBOR MICHIGAN	DESIGNED BY A.W.W	APPROVED BY H. WW
			DRAWN BY	SCALE FULL SIZE
			CHECKED BY	DATE 3/12/48
		PROJECT M-694	TITLE MAGNETRON ASSEMBLY MODEL 3A	
1	3/12/48	CLASSIFICATION	DWG. NO. B-10003A	
ISSUE	DATE			

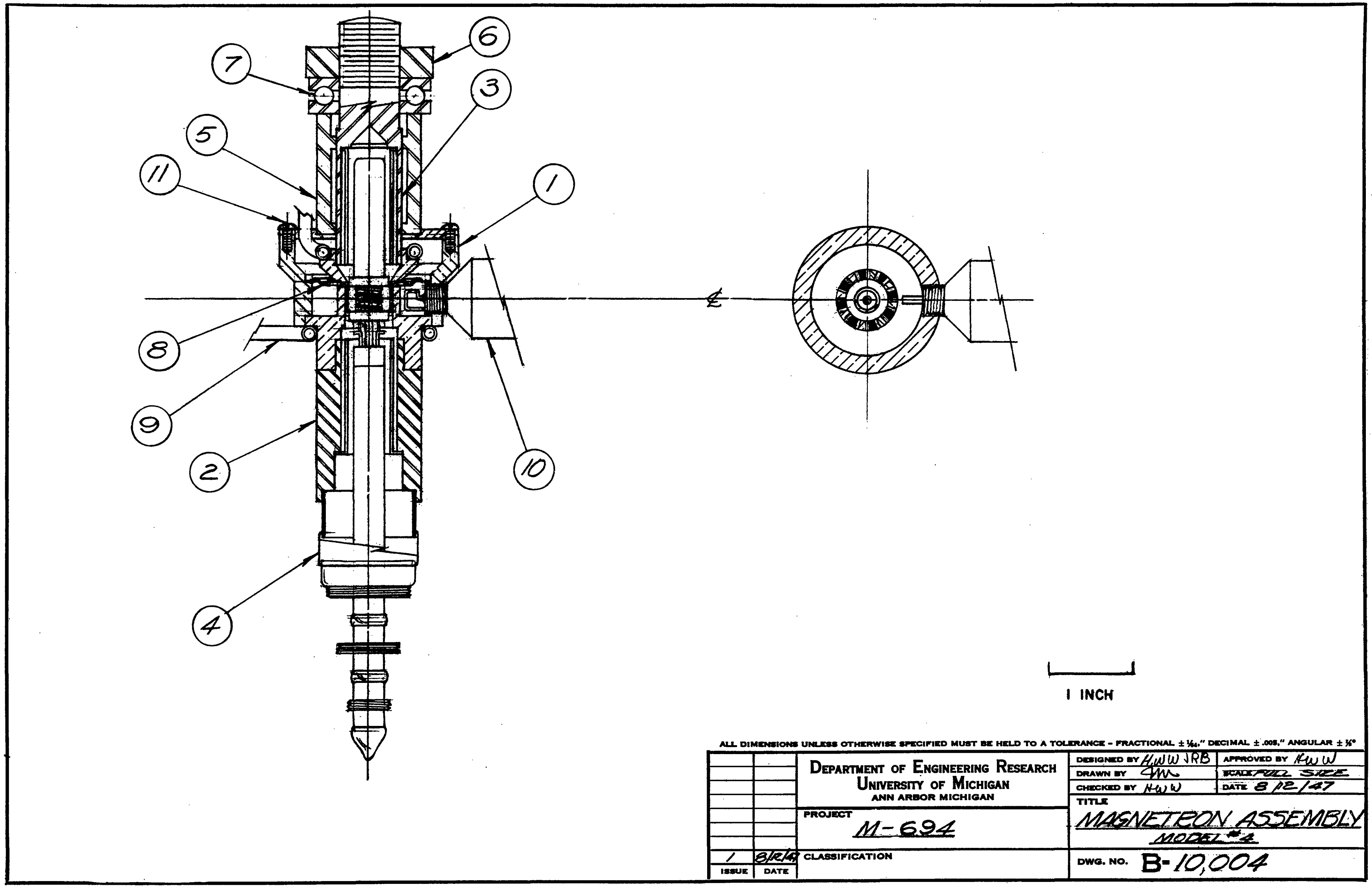
1
2
3
4
5
6
7
8
9
10
11
1 INCH
ALL DIMENSIONS UNLESS OTHERWISE SPECIFIED MUST BE HELD TO A TOLERANCE - FRACTIONAL ± 1/64," DECIMAL ± .005," ANGULAR ± ½°
DEPARTMENT OF ENGINEERING RESEARCH
UNIVERSITY OF MICHIGAN
ANN ARBOR MICHIGAN
PROJECT M-694
CLASSIFICATION
1 8/12/47
ISSUE DATE
DESIGNED BY HWW JRB
APPROVED BY HWW
DRAWN BY
SCALE FULL SIZE
CHECKED BY HWW
DATE 8/12/47
TITLE MAGNETRON ASSEMBLY
MODEL #4
DWG. NO. B-10,004

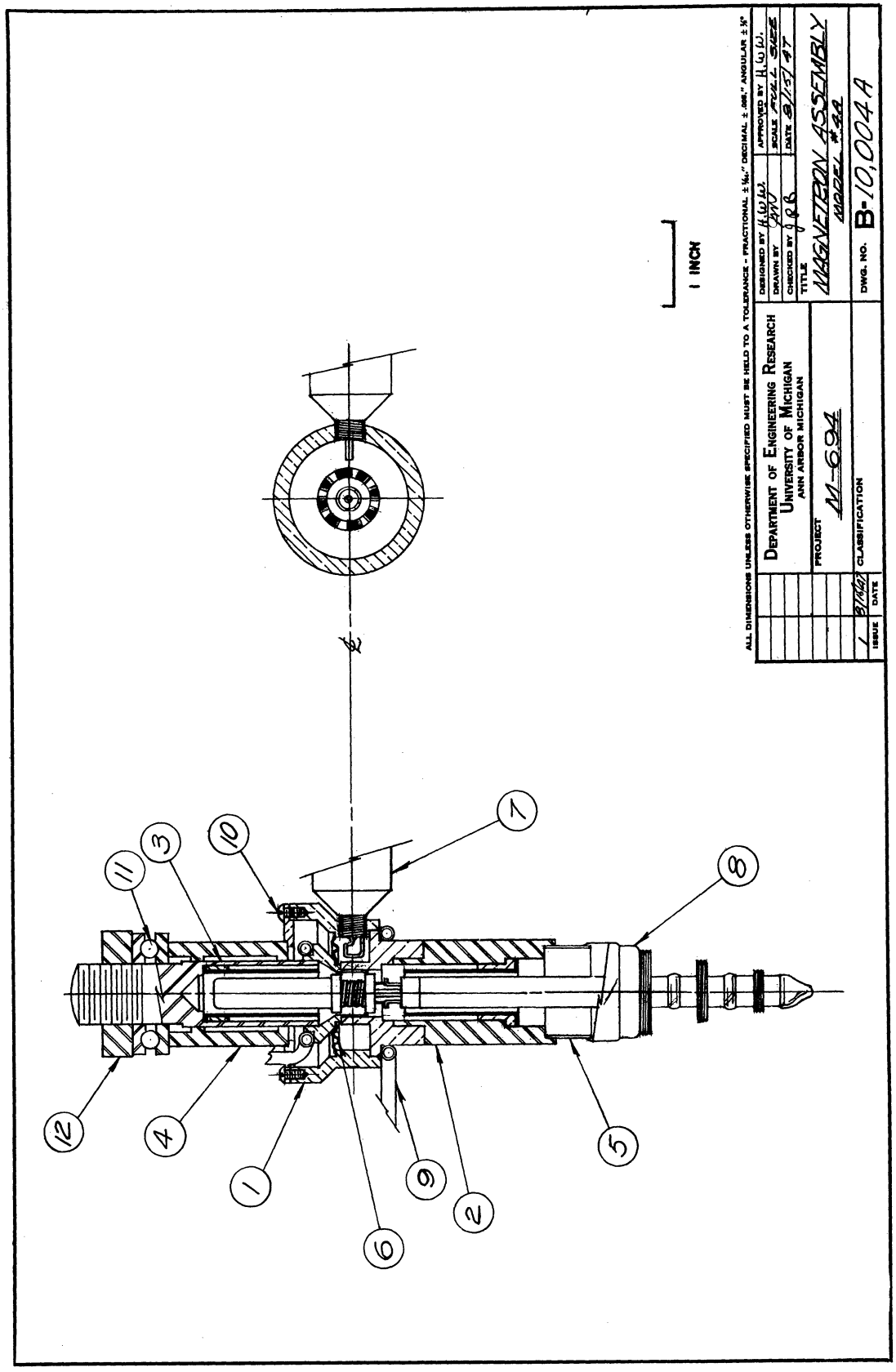

Lithoprinted from copy supplied by author
by
Cushing-Malloy, Inc.
Ann Arbor, Michigan, U.S.A.